4574–4600 *Nucleic Acids Research, 2022, Vol. 50, No. 8* *Published online 14 April 2022*
https://doi.org/10.1093/nar/gkac225

Guanine quadruplexes in the RNA genome of the tick-borne encephalitis virus: their role as a new antiviral target and in virus biology

Jiří Holoubek[1,2,3,†], Klára Bednářová[4,†], Jan Haviernik[1,3], Ivana Huvarová[1], Zuzana Dvořáková[4], Jiří Černý[5], Martina Outlá[6,7], Jiří Salát[1,3], Eva Konkol'ová[8], Evzen Boura[8], Daniel Růžek[1,2,3], Michaela Vorlíčková[4], Luděk Eyer[1,3,*] and Daniel Renčiuk[4,*]

[1]Veterinary Research Institute, Emerging Viral Diseases, Brno CZ-62100, Czech Republic, [2]Department of Experimental Biology, Faculty of Science, Masaryk University, CZ-62500 Brno, Czech Republic, [3]Institute of Parasitology, Biology Centre of the Czech Academy of Sciences, CZ-37005 Ceske Budejovice, Czech Republic, [4]Department of Biophysics of Nucleic Acids, Institute of Biophysics of the Czech Academy of Sciences, Brno CZ-61200, Czech Republic, [5]Faculty of Tropical Agrisciences, Czech University of Life Sciences Prague, CZ-16500 Prague, Czech Republic, [6]Department of Biophysical Chemistry and Molecular Oncology, Institute of Biophysics of the Czech Academy of Sciences, Brno CZ-61200, Czech Republic, [7]National Centre for Biomolecular Research, Faculty of Science, Masaryk University, CZ-62500 Brno, Czech Republic and [8]Institute of Organic Chemistry and Biochemistry of the Czech Academy of Sciences, CZ-16000 Prague, Czech Republic

Received July 02, 2021; Revised March 21, 2022; Editorial Decision March 23, 2022; Accepted March 25, 2022

ABSTRACT

We have identified seven putative guanine quadruplexes (G4) in the RNA genome of tick-borne encephalitis virus (TBEV), a flavivirus causing thousands of human infections and numerous deaths every year. The formation of G4s was confirmed by biophysical methods on synthetic oligonucleotides derived from the predicted TBEV sequences. TBEV-5, located at the NS4b/NS5 boundary and conserved among all known flaviviruses, was tested along with its mutated variants for interactions with a panel of known G4 ligands, for the ability to affect RNA synthesis by the flaviviral RNA-dependent RNA polymerase (RdRp) and for effects on TBEV replication fitness in cells. G4-stabilizing TBEV-5 mutations strongly inhibited RdRp RNA synthesis and exhibited substantially reduced replication fitness, different plaque morphology and increased sensitivity to G4-binding ligands in cell-based systems. In contrast, strongly destabilizing TBEV-5 G4 mutations caused rapid reversion to the wild-type genotype. Our results suggest that there is a threshold of stability for G4 sequences in the TBEV genome, with any deviation resulting in either dramatic changes in viral phenotype or a rapid return to this optimal level of G4 stability. The data indicate that G4s are critical elements for efficient TBEV replication and are suitable targets to tackle TBEV infection.

GRAPHICAL ABSTRACT

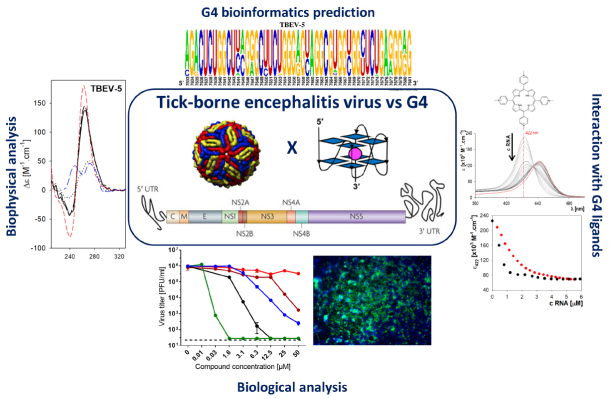

INTRODUCTION

Guanine quadruplexes (G4s) are non-canonical four-stranded conformations of nucleic acids. G4s can be formed

*To whom correspondence should be addressed. Tel: +420 541 517 202; Email: renciuk@ibp.cz
Correspondence may also be addressed to Luděk Eyer. Tel: +420 533 331 911; Email: eyer@vri.cz
†The authors wish it to be known that, in their opinion, the first two authors should be regarded as joint First Authors.

within DNA or RNA when two or more G-tetrads stack on top of each other and coordinate monovalent cations, such as physiological K^+ and Na^+, in the G4 central cavity. Each tetrad is composed of four guanine residues connected through Hoogsteen hydrogen bonds. G4s can fold intramolecularly from a single G-rich strand or intermolecularly through the association of separate strands. The relative orientation of participating guanine tracts defines the parallel, the antiparallel or mixed topology of G4s, which is directly correlated to the conformational state, *anti* or *syn*, of the N-glycosidic bond between the G base and the sugar (1). In the case of RNA, guanosine residues prefer the *anti* conformation of the glycosidic bond which limits the topology of the RNA G4 to parallel types. Potential quadruplex forming sequences (PQS) have been found in the genomes of numerous eucaryotic and procaryotic species (2) and G4 have been shown to act as structural switches of multiple cellular processes (3).

Essential functions for G4 sequences have also been demonstrated in numerous DNA and RNA viruses (4) involving different stages of viral life cycles and the presence of G4 was correlated with the type of infection they cause (5). Regarding DNA viruses, multiple G4 clusters in the herpes simplex virus 1 (HSV-1) genome are required for efficient viral DNA replication (6). Nuclear antigen 1 encoded by the Epstein-Barr virus (EBV) genome binds G4s at the viral replication origin and interacts with the replication complex and with human metaphase chromosomes. This ensures the maintenance of the viral genome throughout mitosis. (7). G4s in the telomeric regions of the human herpesvirus 6 (HHV6) are involved in the mechanism of HHV-6 integration into the telomeres of human chromosomes. This process is considered as one possible mode of virus latency (8). Additional to these DNA viruses, there are several reports of G4s in RNA viruses. The long terminal promoter (LTR) in the HIV-1 genome was demonstrated to form G4 structures that are responsible for promoter activity regulation. In addition, these G4s are also involved in reverse transcription and viral latency establishment (9). G-rich sequences were recently identified in the genomes of two medically important filoviruses, Ebola and Marburg. These sequences are likely involved in filovirus-specific L gene expression (10).

The first evidence of the guanine quadruplex in the *Flaviviridae* family came from studies of the hepatitis C virus (HCV) (11). In the HCV, RNA synthesis was observed to be modulated by G4 formation in the viral negative RNA strand (12). Nucleolin, a host cell protein, recognized another G4 in the HCV genome and this interaction suppressed viral replication and expression (13). HCV RNA quadruplexes were later observed in infected cells using the fluorescent quadruplex-specific thioflavin-T-derivative (14). Fleming *et al*. reported that the RNA genome of the Zika virus (ZIKV) and other members of the genus *Flavivirus* contain conserved RNA quadruplexes (15). Several G4 sequences were discovered in the positive strand of the ZIKV genome: seven of these are conserved within more than 50 flavivirus genomes, indicating an essential role in the flaviviral life cycle. They also suggested that the RNA G4s in the ZIKV genome might serve as a framework for installing epitranscriptomic mark N6-methyladenosine (16). Recently, several novel conserved potential G4s were identified in the ZIKV RNA genome, which were further analyzed by biophysical and biochemical approaches. Treatment of ZIKV-infected cells with G4-binding ligands resulted in the significant inhibition of infectious ZIKV yield, suppression of viral genome replication and viral protein synthesis (17,18). The potential role of G4s as antiviral targets was recently reviewed (19,20).

In this work, we studied the occurrence and structure of potential G4 sequences in the genome of the tick-borne encephalitis virus (TBEV), the most medically important representative of flaviviruses transmitted by ticks. The TBEV is prevalent over large forested areas of Europe and Asia, causing tick-borne encephalitis (TBE) in humans. TBE is a serious and potentially fatal neural infection with an estimated annual number of disease cases of >13 000 (21). The TBEV comprises three main subtypes: Western/European, Siberian and Far Eastern with the possibility of several minor subtypes also existing (22). The TBEV, as a typical flavivirus, is a small (∼50 nm in diameter), enveloped, icosahedral virus (23) that possesses a positive-sense single-stranded RNA genome of ∼11 kb in length. The genome encodes one large open reading frame (ORF) which is flanked by a 5′ and a 3′ untranslated regions (UTR). The 5′ end of the genome is capped and the 3′ end is not polyadenylated. The ORF encodes a single polyprotein co- and posttranslationally cleaved by viral and cellular proteases into three structural (C, prM, and E) and six nonstructural (NS1, NS2a, NS3, NS4a, NS4b and NS5) proteins (21).

Herein, the TBEV genome was investigated for the presence of G4s using multiple bioinformatics, biophysical, and biological approaches. Initially, the genome was examined using available G4-search algorithms to predict the potential formation of G4s directly from the primary structure of RNA sequence and the conservation among different TBEV strains and within the *Flavivirus* genus was explored. Selected quadruplex-forming sites were characterized as synthetic oligoribonucleotides in terms of structure, thermodynamic stability and formation kinetics, by circular dichroism, UV absorption spectroscopy and native polyacrylamide gel electrophoresis. The interactions of the G4 motifs located in the TBEV genome with small molecule-based G4-ligands were assessed by thiazole orange fluorescence displacement assay, titration assays using changes in absorption of ligands upon binding to RNA and G4-stabilization assay. We also investigated whether the formation of G4 affects *in vitro* RNA synthesis by the flaviviral RNA-dependent RNA polymerase (RdRp). The antiviral and cytotoxic properties of selected G4 ligands were studied in cell-based assay systems to demonstrate G4-mediated mechanisms at biological levels. Finally, site-directed mutagenesis was used to introduce conformation-specific mutations into a conserved G4 motif in the TBEV genome in order to assess the growth kinetics, plaque morphology and sensitivity of the mutated viruses to G4 ligands. Our results bring novel insights into the structure and folding of TBEV genomic RNA, which are crucial to understanding the molecular basis of TBEV pathogenesis. This new information can be essential for new antiviral treatments and the development of novel vaccination strategies.

MATERIALS AND METHODS

Bioinformatics analysis

The TBEV strain Neudoerfl reference genome sequence (NC_001672.1, sequence identical to U27495.1), genomic sequences of other TBEV strains, as well as genomes of all viruses of the *Flavivirus* genus, reported in (15), were downloaded from the Nucleotide database of the NCBI. Genome sequence alignments were performed using the MUSCLE algorithm (24) with the default setting embedded in the UGENE package (25). A rough phylogenetic tree was calculated in UGENE using the PHYLIP Neighbour Joining method (F84 model; Transition/Transversion ratio 2; Bootstrapping OFF; Gamma-distribution rates across sites OFF). Potential G4-forming regions selected for further bioinformatics analysis were extracted as multiFASTA files with gaps trimmed.

G4 prediction for the TBEV genome (NC_001672.1) was performed with QGRS mapper (max G4 length = 30 nt; min G-tract length = 2 nt) (26), pqsfinder (max length = 30 nt, min G-tract = 2 nt, loop min len = 1 nt, max bulges = 0, max mismatches = 0) (27), G4Hunter (window size = 20 nt; threshold = 1.49) (28) and G4RNA screener (window size = 20 nt; step size = 5 nt) (29).

G4Hunter scores of extracted regions from aligned genomes in multi FASTA files of members of the *Flavivirus* genus as well as TBEV strains were calculated using the G4HunterTable utility (30) in R studio. RNA sequence logos of the aligned set of 204 TBEV strains were prepared as frequency plots using the 'weblogo' tool (31).

Oligonucleotides

Synthetic RNA oligonucleotides were purchased from Merck (Haverhill, UK) and were desalted and lyophilized by the provider. For clarity, we did not use the standard r(…) notation as most of the oligonucleotides were RNA. Lyophilized oligonucleotides were dissolved in 1 mM sodium phosphate buffer, pH 7 with 0.3 mM EDTA to a 10 mM nucleoside concentration stock solution. The precise concentration of the oligonucleotides used for each experiment was determined from UV absorption at 260 nm in buffer at 90°C using molar absorption coefficients calculated according to our previous work, e.g. (32) and shown in Table 1. All sequences used in this study and their labels are summarized in Table 1.

G4 ligands

Pyridostatin (PDS) (33), hemin (34), bisquinolinium derivative PhenDC3 (35), thioflavin T (ThT) (36), thiazole orange (TO) (37), crystal violet (CV) (38), acridine derivative BRACO-19 (39), hydroxyantraquinone natural compound aloe-emodin (40) and natural alkaloid berberine (41) were purchased from Sigma-Aldrich (Prague, Czech Republic). N-Methylmesoporphyrin IX (NMM) (42,43) and 5,10,15,20-tetrakis-(*N*-methyl-4-pyridyl)porphine (TMPyP4) (42,44) were obtained from Santa Cruz Biotechnology (Heidelberg, Germany). Carboxy pyridostatin (cPDS) (45,46), bisquinolinium derivative 360A (47) and polymerase I inhibitor CX5461 (48) were from MedChemExpress (Stockholm, Sweden). Test compounds were solubilized according to the recommendations of the provider in water or in 100% (v/v) dimethyl sulfoxide (DMSO) to yield stock solutions of desired concentration, usually 10 mM.

Spectroscopy of circular dichroism (CD)

CD measurements were conducted on a Jasco J-815 dichrograph (Jasco Corp., Tokyo, Japan). Presented CD spectra were collected as an average of four measurements between 330 nm and 210 nm with data pitch 0.5 nm at 200 nm min^{-1} acquisition speed. Spectra were measured in 1 cm-pathlength quartz cells (Hellma GmBH, Müllheim, Germany) at 23°C. CD signals are expressed as the difference in the molar absorption $\Delta\varepsilon$ of the left- and right-handed circularly polarized light and the molarity is related to strands. The experimental conditions were changed directly in the cells by adding stock solutions of buffers and the final concentration was corrected for the volume increase. Spectra or values labelled 'after annealing' were observed in the same buffer as the previous ones after heating to 95°C for 5 min and slow linear cooling back to 23°C within 5 h.

Titration experiments using UV absorption

Absorption measurements during titration experiments were conducted in a Specord 250 Plus spectrophotometer (Analytik Jena, Jena, Germany). Whole absorption spectra of RNA with ligand or control were taken from 200 to 700 nm with 1 nm step and 10 nm s^{-1} acquisition speed at 23°C. Two types of titration experiments were performed: (i) for RNA-to-Ligand experiments, 1000 μl of ligands were prepared into 1 cm-pathlength quartz cells to a 4 μM concentration in 1× IC buffer (25 mM sodium phosphate buffer, pH 7, 110 mM KCl, 10 mM NaCl). Twenty consecutive additions of 10 μl of RNA at 40 μM strand concentration in 1× IC buffer were performed, with absorption spectra measurement after each addition. (ii) For the Ligand-to-RNA experiments, 1000 μl of RNA were prepared into 1 cm-pathlength quartz cells to a 4 μM strand concentration in 1× IC buffer. Then 25 consecutive additions of 10 μl ligands at 40 μM strand concentration in 1× IC buffer were carried out, along with absorption spectra measurement after each addition. Absorption spectra were recalculated into molar units with known molar absorption coefficients of ligands.

Fluorescence measurements and fluorescence intercalator displacement assay (FID)

FID assay was performed either with TO, as described in Tran *et al.* (49), or with (ThT, where only the probe and excitation and emission wavelengths were modified. RNA oligonucleotides were pre-incubated in 1× IC buffer for 1 h at 25°C. Two molar equivalents of TO or ThT in the same buffer were added and the mixture was incubated for 1 h at 25°C. Next, five equivalents of ligand were added to each sample and the mixture was incubated for 30 min at 25°C. The total reaction volume was 80 μl with 1 μM RNA, 2 μM TO or ThT and 5 μM tested final ligand concentration. Fluorescence was measured in 96-well opaque microplates

Table 1. Labels, primary sequences and molar extinction coefficients of oligonucleotides used for structural studies in the paper

Label	Sequence	ε [$M^{-1}.cm^{-1}$][a]	Position[b]	Protein
TBEV-1	AAGGUAAGGGGGGCGGUC	194 000	154	Core protein C
TBEV-1mut	AAGAUAAGAGGAGCGGUC	194 900		
TBEV-1b	AAGGUAAGGGGGGCGGUCCCCCUCGA	265 300	154	Core protein C
TBEV-2	UUGGAGUGGGGGCGGAUGUUGGUU	250 700	2447	Envelope / NS1
TBEV-2mut	UUGGAGUGAGUGCGGAUGUUGGUU	243 200		
TBEV-3	AUGGUGGGCACGGAAGGAC	201 400	2863	NS1
TBEV-3mut	AUGGUGAGCACGAAAGGAC	199 500		
TBEV-4	UCGGGGAGGGGGAGGCA	182 400	7382	NS4b
TBEV-4mut	UCGAGGAGUGAGAGGCA	179 900		
TBEV-5	CUGGGGGUAGGCGUGGUGGUU	215 000	7652	NS4b / NS5
TBEV-5mut	CUGUGUGUAUGCGUGUUGGUU	210 700	—	—
TBEV-6	CUGGGAGUUGGAACGAGGUGUGUGGUC	280 300	8440	NS5 (RNA pol)
TBEV-6mut	CUGAGAGUUGAAACGAGUUGUGUGGUC	276 000		
TBEV-7	UUGUGGGGGGAGGCUAGGAGGCGAA	268 000	10653	3′-UTR
TBEV-7mut	UUGUGUAGCGAAGCUAGGAUGCGAA	256 800		
R-psG4	AAUGGGUGGGUGGGUGGGUAA	230 000		

[a]ε calculated for strand using nearest-neighbor model.
[b]Position of the first nucleotide in TBEV reference genome NC_001672.1.

(SPL Life Sciences) at 25°C by Synergy H1 hybrid reader (BioTek) with excitation at 492 nm (TO)/430 nm (ThT) and the emission collected at 533 nm (TO)/480 nm (ThT) and gain set to 100. Each condition was tested in triplicate, fluorescence intensity was averaged and SD calculated. The percentage of TO/ThT displacement was derived similarly as in Carvalho *et al*. (50), using the formula: Displacement (%) = 100 – [100 × (FI – Fb)/(FI_0 – Fb)], where FI stands for fluorescence with ligand, FI_0 for fluorescence without ligand and Fb for fluorescence of background.

Fluorescence measurements of ThT upon interaction with RNA oligonucleotides were performed in a similar way as FID with ThT without addition of the tested ligand.

Temperature-dependent absorption measurements and thermal difference spectra

Temperature melting measurements were conducted in a Varian Cary 4000 spectrophotometer (Varian, Mulgrave, Australia). Whole absorption spectra were taken at each temperature step (1°C) from 230 to 400 nm with a 1 nm step and 600 nm min^{-1} acquisition speed. Four consecutive temperature ramps were run between 23°C and 95°C with 1°C step (alternating denaturation and renaturation processes) and 2 min waiting time at each temperature, giving an average temperature change of 0.25°C min^{-1}. As a blank, a similar cell with only 1× IC buffer was used. Absorbance spectra were recalculated to molar units similarly to CD spectra and molar absorbance at 297 nm was plotted as a function of temperature to give melting and annealing curves. These were dual-baseline corrected with linear baselines fitting pre- and post-melting parts of observed melting curves (51) and melting temperatures (T_m) were calculated as a temperature, where baseline-corrected molar absorbance is equal to 0.5.

Thermal difference spectra (TDS) were calculated as the difference between molar absorption spectra measured at 95°C and at 23°C during the first temperature ramp of the melting experiment in 1× IC buffer.

Viruses and cell cultures

TBEV strains Neudoerfl and Hypr, both members of the West European TBEV subtype, were provided by the Collection of Arboviruses, Institute of Parasitology, Biology Center of the Czech Academy of Sciences, Ceske Budejovice, Czech Republic, http://www.arboviruscollection.cz/index.php?lang=en). All work with infectious TBEV was performed in biosafety level 3 facility at the Veterinary Research Institute, Brno, Czech Republic. Porcine stable kidney (PS) cells, an immortalized cell line widely applied for TBEV isolation and multiplication (52) were used as a model cell line for antiviral and cytotoxicity cell-based assays. All experiments based on the transfection of Infectious Subgenomic Amplicons (ISA) or viral RNA (see below) were performed in BHK-21 cells (ATTC CCL-10), because this cell line is highly susceptible to uptake and/or recombine the transfected nucleic acid (53–55). The cells were cultured in Leibovitz (L-15) medium (PS) and Dulbecco′s modified Eagle′s medium (DMEM) (BHK-21) supplemented with 3% (L15) and 10% (DMEM) newborn calf serum and 100 U/ml penicillin, 100 μg/ml streptomycin and 1% glutamine (Sigma-Aldrich, Prague, Czech Republic). BHK-21 cells were cultivated at 37°C in 5% CO_2, whereas PS cells were cultured at 37°C in a normal atmosphere (without CO_2 supplementation).

Cytotoxicity assay

To determine the cytotoxicity of G4 ligands, PS cells were seeded in 96-well microtitration plates (2×10^4 cells/well) and incubated for 24 h. After incubation, the test ligands were added to the cells in a concentration range from 0 to 50 μM (three wells per compound in two independent experiments) and the treated cells were cultivated for 48 h at 37°C. Cytotoxicity was determined in terms of cell viability using the Cell Counting Kit-8 (Dojindo Molecular Technologies, Munich, Germany) according to the manufacturer's instructions and expressed as 50% cytotoxic concentration (CC_{50}, the amount required to cause a 50% reduction in cell viability).

Virus titer reduction assays

The antiviral efficacy of G4 ligands, which showed a low cytotoxicity for PS cells (PDS, cPDS, NMM, TMPyP4, hemin, 360A, PhenDC3, BRACO-19 and berberine), was initially tested at a single concentration of 50 μM in PS cells using a viral titer reduction assay. The cells were seeded in 96-well plates (approximately 2×10^4 cells per well) and incubated for 24 h to form a confluent monolayer. Following incubation the medium was aspirated from the wells and replaced with 200 μl of fresh medium containing 50 μM of the appropriate G4 ligand (three wells per compound in two independent experiments) and inoculated with TBEV (Neudoerfl or Hypr) at a multiplicity of infection (MOI) of 0.1. DMSO was added to virus-infected cells as a negative control at a final concentration of 0.5% (v/v). Viral titers were estimated from the collected media using a plaque assay after 48-h cultivation. To study the dose-response antiviral effect of the selected G4-binding ligands (PDS, cPDS, NMM, TMPyP4, PhenDC3 and berberine) the same experimental procedure was performed as described above with slight modifications. Growth medium was aspirated from PS cell monolayers, replaced with 200 μl of fresh medium containing the compounds from 0 to 50 μM and TBEV (strains Neudoerfl or Hypr) at an MOI of 0.1 and cultivated for 48 or 72 h at 37°C. Viral titers were determined by plaque assays. Viral titer values obtained from the PS-based antiviral assays at experimental interval 48 h.p.i. were used to construct dose-dependent curves and calculate the 50% effective concentrations (EC_{50}).

Plaque assay

Plaque assays were performed in PS cells to determine TBEV titers as described previously (56,57). Briefly, 10-fold dilutions of TBEV were prepared in 24-well tissue culture plates and the cells were added to each well ($0.6–1.5 \times 10^5$ cells per well). After a 4-h incubation, the suspension was overlaid with 1.5% (w/v) carboxymethylcellulose in L-15 medium. Following a 5-day incubation at 37°C the infected plates were washed with phosphate-buffered saline and the cell monolayers were stained with naphthalene black. The virus titer was expressed as plaque-forming units (PFU)/ml.

Immunofluorescence staining

To measure the G4 ligand-induced inhibition of viral surface antigen expression, a cell-based flavivirus immunostaining assay was performed as previously described (57). Briefly, PS cells were seeded onto 96-well microtitration plates to form a confluent monolayer. After a 24-h incubation, the cells were treated with G4 ligands at concentrations of 0, 10 and 50 μM then simultaneously infected with TBEV strains Neudoerfl and Hypr at an MOI of 0.1 and cultured for 48 h at 37°C. For NMM, concentrations of 0, 10 and 25 μM were used. We did not use NMM at 50 μM due to observable changes in cell morphology and monolayer coherence at this concentration. The experiment was performed in triplicate. After cold acetone–methanol (1:1) fixation and blocking with 10% fetal bovine serum we incubated the cells with a mouse monoclonal antibody targeting the flavivirus group surface antigen (protein E) (1:250; antibody clone D1-4G2-4-15; Sigma-Aldrich, Prague, Czech Republic) and labelled it with an anti-mouse goat secondary antibody conjugated with fluorescein isothiocyanate (FITC; 1:500) by incubation for 1 h at 37°C. The cells were counterstained with 4′,6-diamidino-2-phenylindole (DAPI; 1 μg/ml) for visualization of the cell nuclei and the fluorescence signal was recorded with an Olympus IX71 epifluorescence microscope. The level of viral antigen expression in the presence of G4 ligands was quantified and expressed as a percentage of infected (viral antigen expressing) cells relative to mock-infected cells.

Quantification of viral RNA synthesis

The effect of G4 ligands (concentrations of 0, 10 and 50 μM; for NMM we used 25 μM instead of 50 μM) on viral genomic RNA replication efficacy was studied using quantitative real-time PCR (RT-qPCR). RNA was isolated from growth media supernatants using the QIAmpViral RNA mini kit (Qiagen, Germantown, MD, USA) following manufacturer's instructions. RT-qPCR measurements were performed on the LightCycler 480 II in a 96-well plate block (Roche, Basel Switzerland) using the Advanced Kit for Tick-borne Encephalitis (Genesig, Germantown, MD, USA) and Lyophilized OneStep qRT-PCR (Oasig) following manufacturer's instructions. TBEV copy numbers/μl were calculated from calibration curves based on standards provided by the manufacturer (Genesig, Germantown, MD, USA).

Adhesion assay

The adhesion assay was used to distinguish whether the ligands show an antiviral effect before entering the cell (inhibition of viral adsorption/fusion) or act in the post-entry phase. This assay was performed in PS cells seeded in 6-well plates. Virus inoculum (10^6 PFU/ml, TBEV strain Hypr) was pre-treated with PDS, cPDS, berberine, PhenDC3 (at 50 μM), or NMM (at 25 μM) for 1 h at 37°C then diluted to 100 PFU/ml and used to infect PS cells in 6-well plates for 1 h at 4°C. Following inoculation, the PS cells were washed with PBS three times to remove the non-adsorbed virus and then fresh medium with 1.5% carboxymethylcellulose was added to the cells. After 5 days of incubation at 37°C, the PS cell monolayers were stained with naphthalene black and the plaque count was determined.

Transfection of viral RNA pre-treated with G4 ligands

Viral genome RNA from the TBEV strain Hypr was isolated using a QIAmpViral RNA mini kit (Qiagen, Germantown, MD, USA) following manufacturer's instructions. The isolated RNA (a mixture of viral RNA and carrier RNA from the QIAmpViral RNA mini kit, a total concentration of 50 ng/μl) was incubated with selected G4 ligands i.e. PDS and berberine at 0, 10, 50 and 200 μM or NMM at 0, 10, 25 and 200 μM for 1 h at 4°C. We also intentionally used an extremely high ligand concentration (200 μM) to make the effect as pronounced as possible. The other two concentrations (10 and 25/50 μM) were the same as in the

previous cell-based experiments. The RNA-lipid complex was prepared as follows: 1 μl of TransIT®-mRNA reagent and 1 μl of mRNA Boost reagent from TransIT®-mRNA Transfection Kit (Mirus Bio, Madison, WI, USA) was diluted in 50 μl Opti-MEM medium (Life Technologies) and then mixed with 0.5 μl of isolated RNA pre-treated with the corresponding G4 ligands. After a 5-min incubation at room temperature, the mixture was added to BHK-21 cells and incubated for 24 h at 37°C. Cell supernatant media were then harvested and virus titer was determined by plaque assay.

Expression and purification of RNA-dependent RNA polymerase from Japanese encephalitis virus (JEV RdRp)

The gene encoding JEV RdRp (GeneBank: NP_775674.1) was synthesized as codon optimized for *Escherichia coli* and was cloned into pET28b vector (European Virus Archive goes Global, EVAg) containing N-terminal 6x His followed by TEV cleavage site. The gene was expressed in *E. coli* (BL-21 CodonPlus (DE3)-RIL) and purified using our protocol optimized for viral polymerase (58). Cells were harvested and the pellet was resuspended in a lysis buffer (50 mM Tris–HCl pH 8.0, 20 mM imidazole, 500 mM NaCl, 10% glycerol, 3 mM β-mercaptoethanol) and sonicated (Q700 Sonicator, QSonica). The lysate was removed by centrifugation and the supernatant was incubated with Ni-NTA agarose (Machery-Nagel), washed with lysis buffer and finally the protein was eluted with lysis buffer supplemented with 300 mM imidazole. The 6× His-TEV tag was digested using TEV protease at 4°C overnight. The protein was then further purified by affinity chromatography using a HiTrap Heparin HP column (GE Healthcare), followed by size exclusion chromatography using a Superdex 200 16/600 (GE Life Sciences) in 20 mM Tris pH 8.0, 800 mM NaCl, 10% glycerol, 3 mM β-mercaptoethanol. Fractions containing JEV polymerase were concentrated to 5 mg/ml, flash frozen in liquid nitrogen and stored at –80°C.

Template and primer preparation for polymerase stop assays

DNA single strands (Table S1), containing TBEV-5 and its mutated variants, denoted as *positive*, *negative* and *super-negative* (see below) together with primer binding sites and T7 RNA polymerase promoter, were acquired as synthetic oligonucleotides (Merck). The double stranded form was prepared by two-step PCR (30 cycles, 98°C/10 s denaturation and 45°C/30 s annealing + elongation) using 100 ng of single stranded template, forward (TAATACGACTCACTA) and reverse (GCGTGTCTCG) primers and PrimeStar GXL polymerase (Takara Bio Inc). PCR products were purified by QIAquick columns (Qiagen) into 50 μl of elution buffer. RNA templates (Figure 7A) were prepared from the PCR products above using a HiScribe T7 In Vitro Transcription Kit (New England Biolabs) according to the provider protocol with 8 μl of the PCR product as a template. RNA was purified using a Monarch RNA Cleanup Kit (New England Biolabs). Primers (DNA d(GCGTGTCTCG) for SuperScript IV and RNA GCGUGUCUCG for JEV RdRp) and DNA template single strands (see above) were labelled by ^{32}P using γ-^{32}P-ATP and T4 polynucleotide kinase (New England Biolabs). Labelled DNA was purified using CentriSpin columns (Princeton Separations) and the specific activity was measured.

Reverse transcription by SuperScript IV

RNA templates (0.5 μM) were pre-incubated in SuperScript IV buffer (ThermoFisher Scientific) together with ^{32}P-labelled DNA primer (0.1 μM), dNTP mix (1 mM each) and 50, 10 or 2 μM of selected G4 ligands in total volume of 10 μl for 3 min at 75°C. Samples labelled CTRL were prepared in absence of G4 ligands. Samples were then slowly cooled down to room temperature over 2 h. 0.4 μl of SuperScript IV reverse transcriptase (ThermoFisher Scientific) was added and the mixture was incubated for 60 min at 37°C. Reaction was stopped by adding 0.5 μl of 2 M NaOH and by heating for 5 min at 95°C, which also ensured alkaline hydrolysis of template RNA.

Synthesis of complementary strand by JEV RdRp

RNA templates (0.25 μM) were pre-incubated in JEV RdRp buffer (5 mM Tris, pH 7.4, 10 mM DTT, 0.5% Triton X-100, 1% glycerol) supplemented with 2 mM $MnCl_2$ and 50 mM KCl, together with ^{32}P-labelled RNA primer (0.05 μM), NTP mix (1 mM each) and 50, 10 or 2 μM of selected G4 ligands in total volume of 20 μl for 3 min at 75°C. Samples labelled CTRL were prepared in absence of G4 ligands. Samples were then slowly cooled to room temperature over 2 h. 0.5 μl of 7 μM JEV RdRp was added and the mixture was incubated for 120 min at 37°C. $MnCl_2$ was used instead of the natural $MgCl_2$ cofactor because it substantially increases the activity of the recombinant flaviviral polymerases under the *in vitro* conditions, as reported (59–61).

Denaturing PAGE of polymerase products and products quantification

The generated DNA or RNA was purified by ethanol-acetate precipitation, then dissolved in 2 μl of loading dye (bromphenol blue and xylene cyanol in formamide), denatured by heating for 5 min at 95°C and 1.5 μl (around 130 kcpm) was loaded onto a pre-heated 40 cm denaturing polyacrylamide gel (16% acrylamide mixture 29:1 mono:bis, 7 M urea, 1× TBE). Electrophoresis was performed in 1× TBE for 90 min at 45 W. The gel was then exposed to a Phosphor imager screen for 15 h (SuperScript IV) or 2 h (JEV RdRp) and the image was digitalized by a Typhoon FLA 9500 device. Observed lanes were background corrected by subtracting the signal density average from the no-label region and the integrated density of each lane was normalized to the same value. Relative fraction of full products in each lane, corresponding to a manually chosen part, was calculated. Relative ratio (in %) between tested samples and CTRL was calculated.

Site directed mutagenesis of the TBEV-5 region

We used a reverse genetics system derived from TBEV (strain Hypr) to construct recombinant TBEV bearing

conformation-specific mutations in the TBEV-5 sequence located in NS4b/NS5 genes. This reverse genetics system was based on the generation of infectious subgenomic overlapping DNA fragments that encompass the entire viral genome as previously described (53–55). Three de-novo synthesized DNA fragments cloned into a pUC57 or a pC11 (GenScript, Piscataway, NJ, USA) cover the following parts in the TBEV genome: fragment I (nucleotide position 1 to 3662), fragment II (nucleotide position 3545 to 8043), and fragment III (nucleotide position 7961–11 100). The first and last fragments are flanked respectively in 5′ and 3′ with the human cytomegalovirus promoter (pCMV) and the hepatitis delta ribozyme followed by the simian virus 40 polyadenylation signal (HDR/SV40pA).

Fragments I, II and III were used as templates to generate the overlapping amplicons following the original ISA method (53). Unmodified primers (Table S2) were used to generate three unmodified amplicons (i.e. production of wild-type virus). Mutated primers located on the targeted region (TBEV-5) of fragment II (Table S2) were used to generate two mutated amplicons, i.e. fragment IIa and IIb; these mutated fragments together with unmodified fragments I and III were used to produce three mutated viruses, denoted as the *positive* (T7653G/G7656A/T7659G/T7665G/T7671G), *negative* (G7656A/G7662A/G7677A), and *super-negative* (G7656A/G7662A/G7670C/G7677A) TBEV mutants (Figure 10B). In comparison with wild-type (*WT*), the *positive* G4-specific TBEV mutant was designed to fold a highly stabilized G4 in the TBEV-5 sequence, whereas the *negative* and *super-negative* mutants had a decreased or completely eliminated ability to form G4 in TBEV-5. ISA fragment amplification and BHK-21 transfection were performed, as described previously (55). Cell supernatant media were then harvested and titers of the recombinant viruses were determined by plaque assay. The presence of mutations in the genome of the obtained mutant viruses was verified by sequencing (Sanger method).

Growth kinetics of recombinant G4-specific TBEV mutants

To evaluate the growth kinetics of the obtained G4-specific TBEV mutants, PS cells incubated for 24 h in 96-well plates were infected with the recombinant wild-type virus or with the *positive*, *negative* or *super-negative* TBEV mutants at an MOI of 0.1. The growth kinetics of the *positive* TBEV mutant was further compared with that of the wild-type virus at a 10-fold lower MOI (0.01). The growth medium was collected from the wells daily on days 1 to 7 p.i. (three wells per interval). Viral titers (expressed as PFU/ml) were determined by plaque assay and used to construct TBEV growth curves. Plaque assays were also used to compare the plaque morphology of the mutated TBEV with that of the wild-type virus. After a 168-h cultivation in PS cells, viral RNA was isolated as described above and the presence of conformation-specific mutations in the TBEV-5 region of the individual mutated viruses verified by the Sanger sequencing method.

Sensitivity studies of G4-specific TBEV mutants to G4 ligands

In order to study the sensitivity / resistance of the recombinant viruses mutated in the TBEV-5 region to the selected G4 ligands, 200-μl portions of fresh medium containing PDS or berberine at concentrations ranging from 0 to 50 μM were added to PS cell monolayers, infected with TBEV wild-type or with mutated variants (the *positive*, *negative* and *super-negative* TBEV mutants) at an MOI of 0.1, and incubated for 24 and 48 h. The medium was then collected from the wells and the viral titers were determined by plaque assay. The obtained viral titer values were used to construct dose-response curves, to assess the replication capacity of the mutated viruses in the presence of PDS or berberine and to compare the replication fitness of G4-specific TBEV mutants with that of the wild-type virus.

RESULTS AND DISCUSSION

Identification of potential G4 sites in the TBEV genome and its complement

The TBEV genome consists of one molecule of RNA, i.e. a single-strand, with a positive (coding) polarity that directly serves as a template for viral genome transcription and polyprotein translation. For purposes of G4 as a translation regulator or as a structural element in genome organization, only the coding strand needs to be analyzed. However, the negative strand is formed later in the viral life cycle to serve as a template for genome strand amplification; thus, the negative strand-G4 might influence viral RNA replication. Therefore, we analyzed the presence of potential G4 motifs in both positive (coding) and negative (anticoding, complementary) TBEV genome RNA strands to directly obtain sequences with potential G4-mediated function for subsequent biophysical and biological studies and to show their conservation, which is considered a strong indicator of the G4 role. Overall analysis of G4 content in all known viruses and its relationship to virus pathogenicity was already reported (5,62). In contrast to these studies, we employed a combination of several G4-search algorithms, namely QGRS mapper (26), pqsfinder (27), G4 Hunter (28) and G4RNA screener (29), because various search algorithms identify quadruplexes using different conditions such as optimal G4 pattern (QGRS mapper, pqsfinder) or G to C ratio and tract length (G4Hunter, G4RNA screener) (63). Briefly, pattern-based algorithms (i) identify preferentially intramolecular G4, but (ii) cannot penalize cytosines that outcompete guanines in WC-pairs instead of Hoogsteen-hydrogen bonds in guanine tetrads; (iii) GC-based algorithms compensate for cytosines, but (iv) give a high score to oligo-G sequences unable to form intramolecular G4. None of the algorithms will automatically discard G4-prone sequences neighboring C-blocks that might outcompete G-blocks in Watson–Crick base pairs, as evaluated for the TBEV-1b sequence below, with sufficient efficacy and manual check of the hits needed to be performed. The analysis was performed using the genome sequence of the TBEV strain Neudoerfl (NCBI ref seq. NC_001672.1 or U27495.1, sequences are identical), which consists of 11 141 nt with 31.73% guanine and 22.04% cytosine content.

With a 40-nt maximum total length in QGRS mapper and pqsfinder, we did not observe any region within positive or negative RNA able to theoretically form a three or more-tetrad intramolecular quadruplex. Two-tetrad monomolecular RNA quadruplexes were predicted to be stable by theoretical methods (64) and our ongoing research supports their existence. It should be noted that the formation of their DNA counterparts strongly depends on additional stabilizing elements (capping base pairs or triads) resulting from primary sequence (65). However, direct experimental evidence of such RNA quadruplexes still has not been obtained. In the positive strand we observed 47 non-overlapping hits with QGRS mapper at threshold 19; 18 hits with pqsfinder at threshold 26; 18 hits with G4 Hunter at threshold 1.49 and 14 hits with G4 Screener (Figure 1). For hits identified by G4 Screener, we selected sequences with a score above the respective threshold (40 for cGcC, 1.49 for G4Hunter and 0.9 for G4NN) for at least two out of the three incorporated algorithms. The thresholds, dimensionless relative values, were set based on algorithm author recommendations or empirical comparisons with experimental data. In most cases, sequences predicted by G4Hunter or G4RNA Screener were predicted by QGRS mapper but not vice versa. We observed six sequences that were predicted by all four algorithms. Only one of them, TBEV-5, overlaps with some of the G4 sequences identified to be conserved within the genus *Flavivirus*, namely with NS5-A (15). We took all six predicted sequences for subsequent studies together with the TBEV-3 sequence which was predicted only by pattern-based algorithms. The TBEV-1b sequence is a 3′-extended variant of TBEV-1 that includes a native neighboring five-cytosine block. The observed sequences are listed in Table 1.

With the same search algorithms settings and thresholds, applied on the complementary i.e. negative strand, we observed only four non-overlapping hits with QGRS mapper, one hit with pqsfinder that overlaps with a QGRS mapper identified hit, one hit with G4 Hunter that is distinct from QGRS mapper/ pqsfinder hits and one with G4 Screener, overlapping the G4 Hunter hit (Supplementary Figure S1). Thus, even under relatively mild conditions, we did not identify any potential quadruplex-forming site within the sequence complementary to the TBEV reference genome.

Conservation of TBEV-selected G4 sites within the *Flavivirus* genus and among TBEV strains

We then checked the conservation within the *Flavivirus* genus (Figure 2), in terms of propensity to form G4, of regions both identified by us and those previously reported (15). G4 conservation was evaluated using the G4HunterTable utility (30), with extended sequences of interest selection on aligned genomes (see MM section). Sequences identified in (15) were taken as reported in associated SI, leading to lengths between 80 and 130 nucleotides. Sequences identified by us in the TBEV reference genome were extended by 20 nucleotides at each end to give a final length between 60 and 70 nt. We chose this approach, instead of selecting the part of the sequence with the highest score, to integrate the potential effect of additional neighboring G- and C-tracts. Sequence length is also the reason why the values reported in Figure 2 are lower than the 1.49 score, generally accepted for stable G4. The varying lengths of selected sequences limits the possibility of direct comparison between various sequences and so only one sequence between different species or strains should be compared.

All the potential G4 regions identified previously (15) have a more or less conserved propensity to form G4 among the whole *Flavivirus* genus. Out of the G4 regions identified by us on a reference TBEV genome (NCBI ref seq. NC_001672.1) only the extended variant of TBEV-5 has relatively conserved G4-formation tendency among the whole *Flavivirus* genus (Figure 2). The G4-propensity of regions corresponding to other TBEV regions is significantly conserved only among tick-borne flaviviruses. TBEV-7 is located within the variable region of the 3′ UTR, which is not present in all TBEV genomes, and its propensity to form G4 is more or less independent of phylogeny within the *Flavivirus* genus. The region around TBEV-3 shows a G4Hunter score close to zero due to the extension that leads to the incorporation of the C_6 tract at 5′ proximity to the G4 site. G4Hunter scores of regions around TBEV-1 are reduced as well, compared to those observed above in a search mode, for a similar reason.

Similar to our approach to members of the *Flavivirus* genus above, we aligned 204 genomes of TBEV strains, prepared a rough phylogenetic tree and followed the propensity to form G4 of regions identified by us by calculating the G4Hunter score (Figure 3B). Sequences of extended TBEV regions, with a frequency of individual nucleotides in the TBEV set at specific positions, represented as RNA sequence logos, are shown in Figure 3A. The significant differences in G4Hunter scores are often the result of single nucleotide substitutions mostly inside contiguous G (negative effect on G4Hunter score) or C (positive effect on G4Hunter score) tracts. A significantly higher G4Hunter score for TBEV-4 in the European TBEV strains, especially compared with the Siberian subtype, is given by the presence of G or A at positions 7386 and 7392 (NCBI ref seq. NC_001672.1), potentially altering the G4 formation probability. Contrastingly, the lower G4Hunter score observed for the region around the TBEV-1 site of European strains is due to C occurring at positions 149 and 173 of the reference genome. The Far East and Siberian strains have in one or both positions U. In this case, the potential effect of particular nucleotides at the respective positions is not directly mediated by altering G4 but by altering the cytosine tract potentially outcompeting the guanines from G4 to a hairpin structure. These two effects of nucleotide variability at specific positions might quantitatively differ in real RNA: G4 is probably more sensitive to a disrupted continuous G4-tract than Watson-Crick base pairs-stabilized hairpin to disruption of continuous C-tract. In the case of the TBEV-5, used for subsequent interaction studies (see below), the dominant part of the variability in G4hunter score among TBEV strains is given by G/A substitutions disrupting two G-tracts, one in the middle of the studied region and one at 3′ end (Figure 3A).

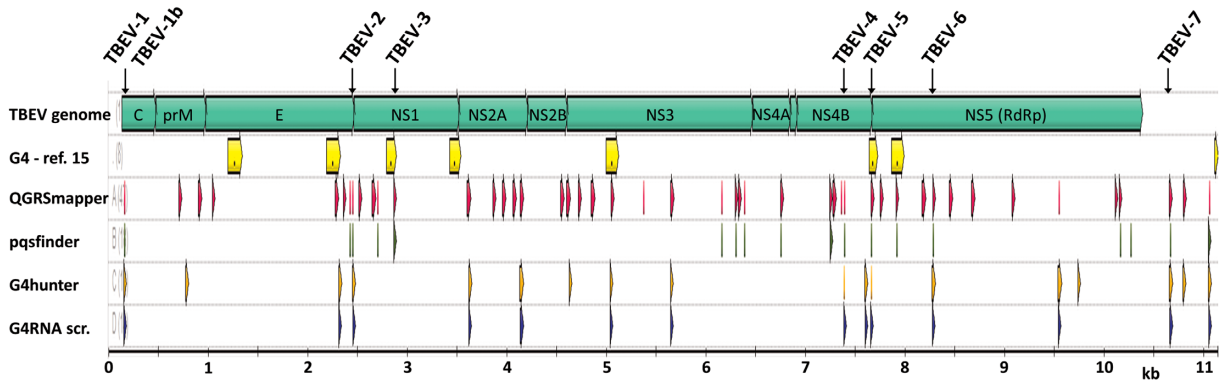

Figure 1. Localization of G4 (black labels with arrows on top) in tick-borne encephalitis virus (TBEV) genome (NC_001672.1) predicted using QGRS mapper (red), pqsfinder (green), G4 Hunter (orange) and G4 RNA Screener (blue). Yellow arrows in the second lane represent conserved G-rich regions reported in (15).

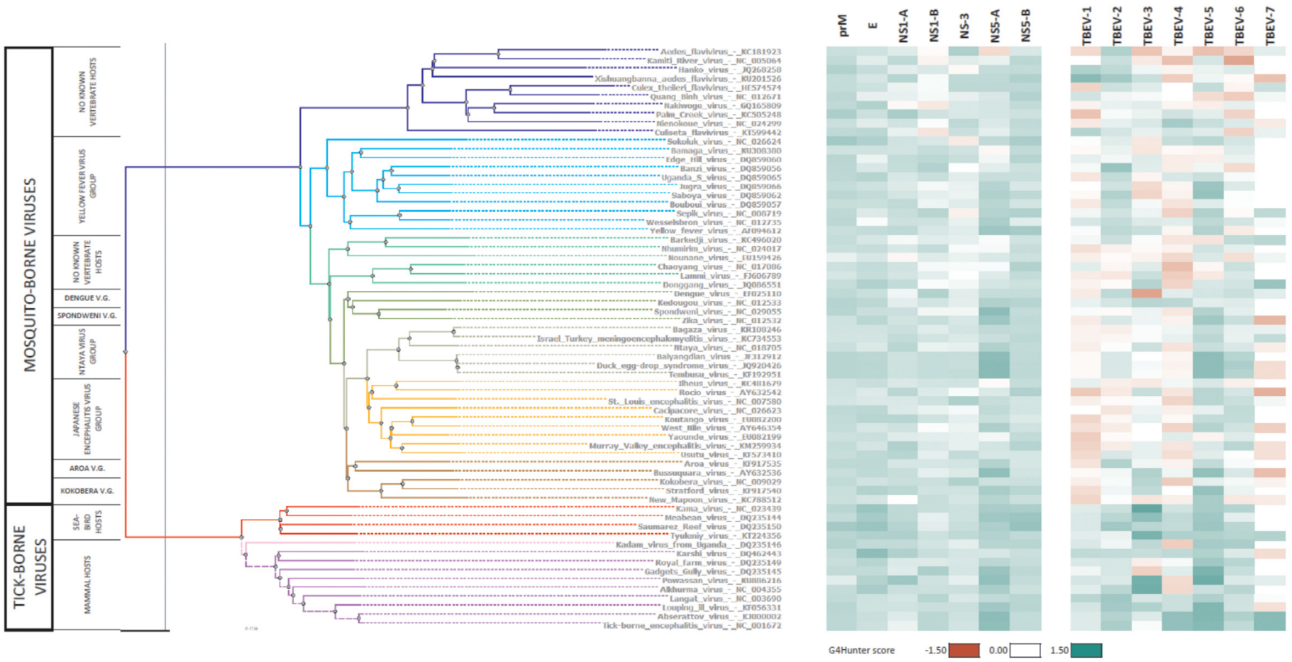

Figure 2. Phylogenetic tree of Flavivirus genus with distinguished main subgroups (left) and heat map representing G4-scores (right), calculated using G4HunterTable, for conserved potential G4 fragments identified by Fleming *et al.* (15) (first set) and by us (second set). Missing values for TBEV-7 correspond to genomes with missing primary sequence of this region in the database. The color coding ranges from red (score -1.5) through white (score 0) to green (score 1.5).

Biophysical properties of selected TBEV G4

Next, we experimentally verified the G4 formation of RNA sequences identified in the previous chapter on synthetic oligonucleotides using CD and UV absorption spectroscopy and native PAGE. As a positive control oligonucleotide that forms regular intramolecular three-tetrad parallel G4, we chose the sequence AAUGGGUGGGUGGGUGGGUAA (R-psG4), giving CD spectrum with a dominant positive peak at 263 nm with molar CD values around 180 M^{-1} cm^{-1} and negative CD peak around 240 nm, indicating parallel G4 (Figure 4). R-psG4, however, does not melt in 1× IC buffer below 90°C and the absorbance remains almost constant during temperature increase (Supplementary Figure S2). For each TBEV oligonucleotide, we also designed a negative control of the same length with several guanines substituted by other bases (Table 1). All seven TBEV sequences (Table 1) produced in 1× IC buffer CD spectra with a positive peak around 263 nm (Figure 4A, C). The CD spectra of the TBEV-4 and to some extent also TBEV-7 correspond to the positive control and the spectra of TBEV-1, 2, and 5 have a similar shape but are reduced in the dominant positive peak at 263 nm. All these spectra significantly differ from that observed in low salt conditions (1mM sodium phosphate buffer, pH 7), where we do not expect formation of any stable secondary structure, especially a guanine quadruplex. The addition of 1× IC buffer thus induces some kind of conformational change that corresponds to the formation of a parallel quadruplex. The negative controls of TBEV-1,

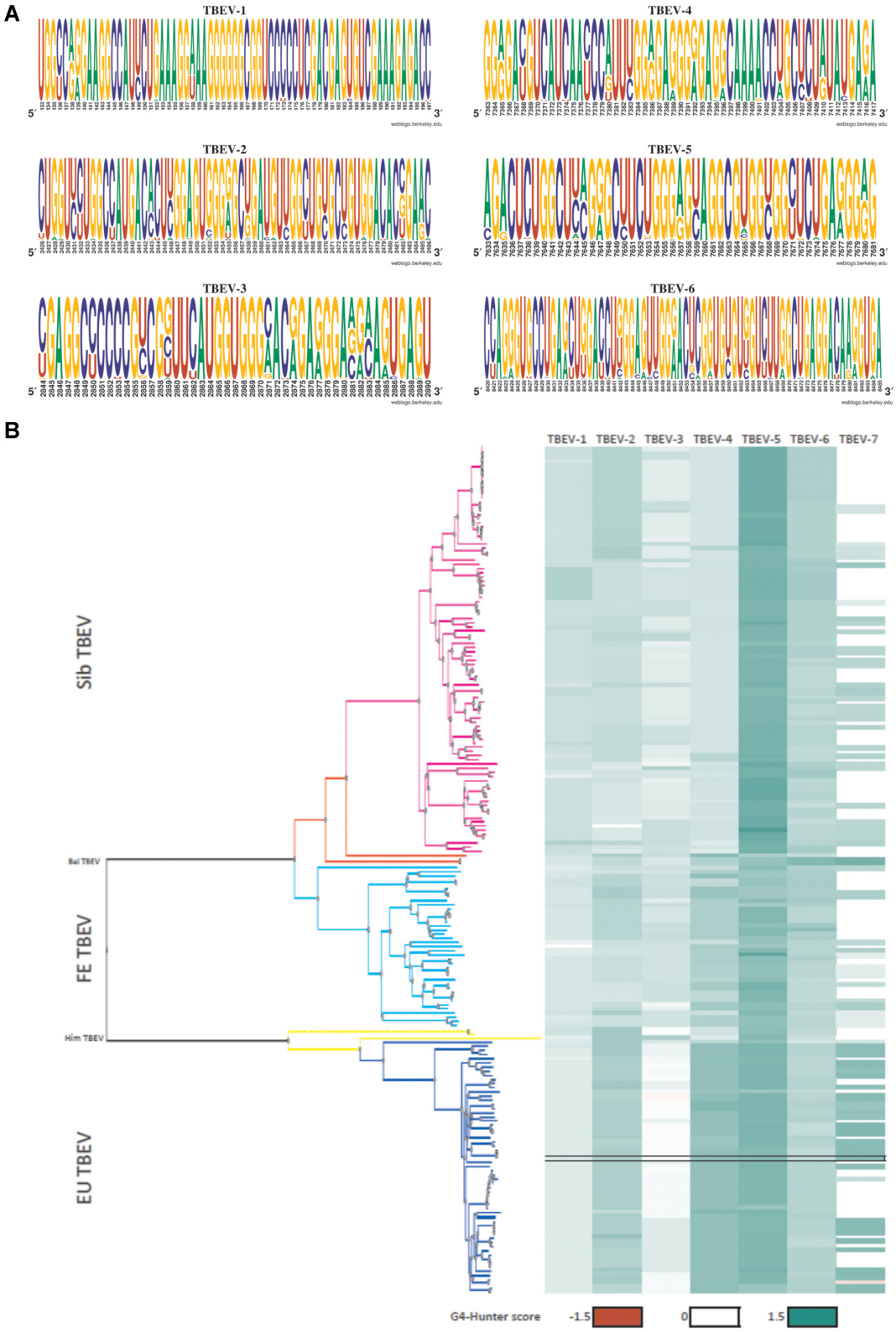

Figure 3. A) RNA sequence logos of the aligned set of 204 TBEV strains were prepared as frequency plots using the 'weblogo' tool (31). TBEV-7 sequence-based logo is not shown as only part of the TBEV strains contains this region. B) Phylogenetic tree of TBEV variants with distinguished main subgroups (left) and G4-scores (right), calculated using G4HunterTable, for conserved potential G4 fragments identified in chapter 3.1. Missing values for TBEV-7 correspond to genomes with missing primary sequence of this region in the database. The darker the green, the higher the G4 score. Reference sequence NC_001672.1 is highlighted.

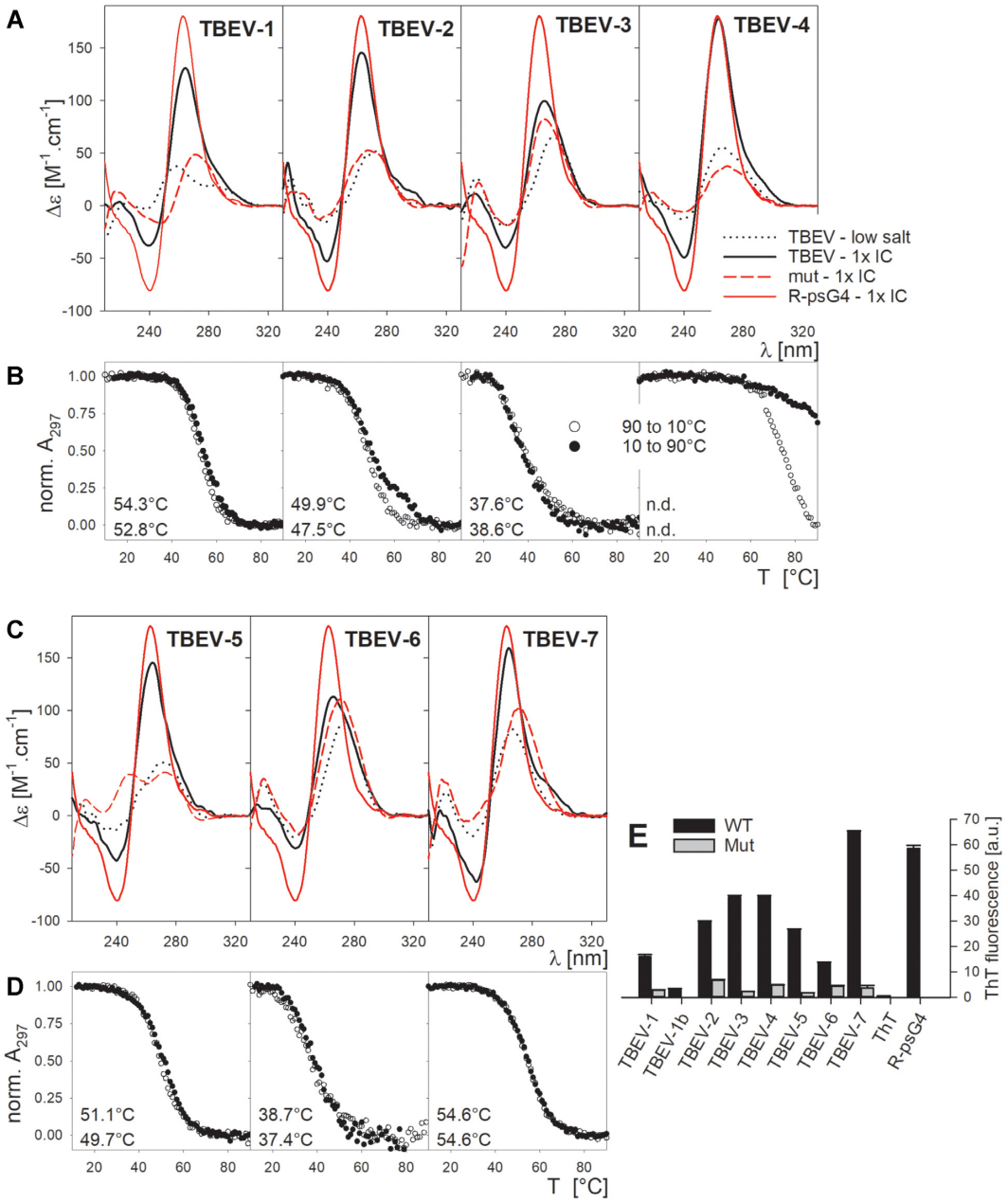

Figure 4. CD spectra (**A**, **C**), denaturation/renaturation curves (**B**, **D**) and fluorescence upon incubation with thioflavin T (**E**) of TBEV and control oligonucleotides. (A, C) CD spectra were measured in 1 mM sodium phosphate buffer, pH 7 (dotted black) and in 1× IC buffer (solid black). Red solid CD spectra correspond to reference oligonucleotide R-psG4. Red dashed CD spectra correspond to mutated variants of particular TBEV sequences. (B, D) Renaturation (empty circles) and denaturation (full circles) curves expressed from the absorbance at 297 nm, normalized to 0–1 scale using dual-baseline correction. Observed Tden/Tren are shown. n.d. – values could not be determined. E: Fluorescence (in arbitrary units) of thioflavin T (ThT) upon incubation with TBEV oligonucleotides and their mutated variants in 1× IC buffer at room temperature.

2, 4, 5 and 7 provide CD spectra with significantly lowered 263 nm positive peaks with amplitudes close to the ones of wild-type sequences in low salt conditions (Figure 4A, C). CD spectra of TBEV-3 and TBEV-6 in 1× IC buffer have a low positive peak at 263 nm, differing in shape from the positive control, and the spectra are close in shape and amplitudes both to those observed in 1mM sodium phosphate buffer and to the respective negative controls. We suppose that there was only a limited formation of G4 for these oligonucleotides at the conditions we used, thus the TBEV-3 and TBEV-6 are not suitable sequences for subsequent analyses. G4 formation of all wild-type sequences is supported by the sigmoidal melting profiles observed at 297 nm by absorption spectroscopy, from which melting temperatures were calculated (Figure 4B, D). The melting profile of TBEV-4 is, however, incomplete, due to extreme stability of the TBEV-4 quadruplex and the melting temperature could not be calculated. Such sigmoidal profiles are missing for the negative control oligonucleotides in the same conditions (Supplementary

Figure S3). All sequences with a high positive peak at 263 nm i.e. TBEV-1, 2, 4, 5 and 7, have melting temperatures close to or above 50°C and a significant negative TDS band at 297 nm, typical for some unusual secondary structures of nucleic acids including guanine quadruplexes (Supplementary Figure S4). TBEV-3 and TBEV-6 have melting temperatures much lower and at ambient temperature a significant fraction of unfolded oligonucleotides might exist (Figure 4B, C). Also, their thermal difference spectra show only a small negative peak around 297 nm, compared to other TBEV G4 supporting the reduced G4-formation propensity (Supplementary Figure S4). TBEV-2 and especially TBEV-4 show hysteresis between melting and annealing curves, indicating the presence of intermolecular G4 rather than a slowly forming intramolecular species. Native polyacrylamide gel electrophoresis (Supplementary Figure S5) provides smeared bands for most of the wild-type variants, indicating a mixture of different species in fast dynamic equilibrium. In the case of TBEV-2 and TBEV-4 the fraction of intermolecular species is much more significant, which makes them unsuitable for subsequent analyses. Based on the results of CD and melting experiments we expect that the negative controls do not form any stable secondary structure and thus they migrate as monomolecular species according to their length. The dominant bands of all wild-type oligonucleotides migrate either faster or at the same speed as the respective negative controls, indicating the formation of monomolecular species. For TBEV-6 we observed two electrophoretic bands corresponding to the monomolecular species. We assigned one band to G4 and the other to an unfolded species. All oligonucleotides mentioned above induce ThT fluorescence upon co-incubation, supporting G4 formation and no significant ThT fluorescence was observed upon interaction with any negative control oligonucleotide (Figure 4E). The ThT fluorescence intensity positively correlates with the stability of G4 and with the ability to form a monomolecular structure. As we mentioned in the first chapter of the Results section, the presence of a neighboring cytosine tract close to the potential quadruplex forming site might reduce the G4 formation ability, which might not be reflected by G4-search algorithms. We thus selected a 3′ extended variant of TBEV-1 (TBEV-1b) involving a native five-cytosine block close to the G4 (Table 1). TBEV-1b provides a high positive CD peak around 265 nm of similar amplitude as the positive control, but at 210 nm provides a significant negative CD signal that was not observed for any of the above-mentioned wild-type oligonucleotides (Supplementary Figure S6). Such a shape of CD spectrum is usually attributed to the presence of double-helical DNA or RNA A-form (66). TBEV-1b does not provide a sigmoidal melting profile at 297 nm, typical for guanine quadruplexes, but we also did not observe a clear sigmoidal melting profile of TBEV-1b around 260 nm indicating the melting of an A-form structure (Supplementary Figure S6). TBEV-1b does not induce significant ThT fluorescence, which supports the absence of G4 formation. This 3′ extended variant of TBEV-1 therefore does not form guanine quadruplexes, however, we cannot confirm our hypothesis that the neighboring cytosine tract might outcompete guanines necessary for G4 formation into an alternative A-DNA structure. The inability of TBEV-1b to form G4 might thus be the result of a destabilizing effect of the significant 3′ sequence extension, irrespective of cytosine content, when compared to TBEV-1.

For subsequent studies, we chose fragment TBEV-5 because (i) TBEV-5 is localized in the part of the genome coding viral NS5 protein with methyltransferase and RNA-dependent-RNA-polymerase activities, both crucial for TBEV RNA genome replication; (ii) TBEV-5 is present and conserved not only among various TBEV strains but also among the members of the *Flavivirus* genus (while TBEV-7 is missing for some strains); (iii) TBEV-5 forms a stable (in contrast to TBEV-3 or TBEV-6) mainly monomolecular (in contrast to TBEV-2 or TBEV-4) quadruplex and (iv) TBEV-5 is not adjacent to any cytosine-rich tract which could potentially disrupt G4 formation (in contrast to TBEV-1).

Interaction of TBEV-5 and its non-G4-forming variant with known G4 ligands

Next, we studied the interaction of TBEV-5 with several reported G4 ligands, namely *N*-methyl mesoporphyrin IX (NMM) (42,43), TMPyP4 (42,44), ThT (36), CV (38), TO (37), CX-5461 (48), 360A (47), PDS (33), cPDS (45,46), PhenDC3 (35), hemin (34), berberine (41), BRACO-19 (39) and aloe-emodin (40). We first used the TO fluorescence displacement assay (37,49), further accompanied by absorption spectroscopy and G4 stabilization assay (Figures 5 and 6). The combination of several assays was used because (i) the ligands might have different modes of interaction with G4, which could influence the results of the FID assay; (ii) for absorption titration, only several ligands give suitable absorption bands that are not affected by RNA presence, i.e. are localized at wavelengths longer than 310 nm and (iii) vice versa, some ligands absorb around 297 nm, which affects the G4 stability determination.

The FID assay was initially performed at 1 μM RNA, with either TBEV-5 or its non-G4 variant TBEV-5mut, 2 μM TO and 5 μM tested ligand. It should be noted that we observed a significant fluorescence of TO in the presence of TBEV-5mut, reaching around 40% of the TO fluorescence in the presence of TBEV-5 (Supplementary Figure S7A). This indicates low selectivity of TO for G4 structure, at least in the case of RNA G4. Moreover, TO probably causes G4 distortions as shown by CD at 5-time excess of TO to RNA (Supplementary Figure S7B). For comparison, we performed an FID assay also with ThT as a probe. ThT is very selective for G4, with only minimal fluorescence in the presence of TBEV-5mut, and neither distort existing G4 of TBEV-5 nor induce G4 formation by TBEV-5mut. For most ligands, the results of the FID assay with TO and ThT are comparable (Figure 5A). For TMPyP4, 360A and PhenDC3, we observed almost 100% displacement of the probe, indicating excellent TBEV-5 binders. BRACO-19 displaces 60–80% of the probe, 50–70% displacement was observed for NMM and 20–40% for CV, CX-5461, PDS, cPDS and hemin. Aloe-emodin did not significantly displace ThT. Generally, ThT is displaced to a greater extent than TO. Interestingly, berberine displaced around 50% of ThT but did not displace TO. The reciprocal experiment showed that TO almost entirely displaces ThT in TBEV-5

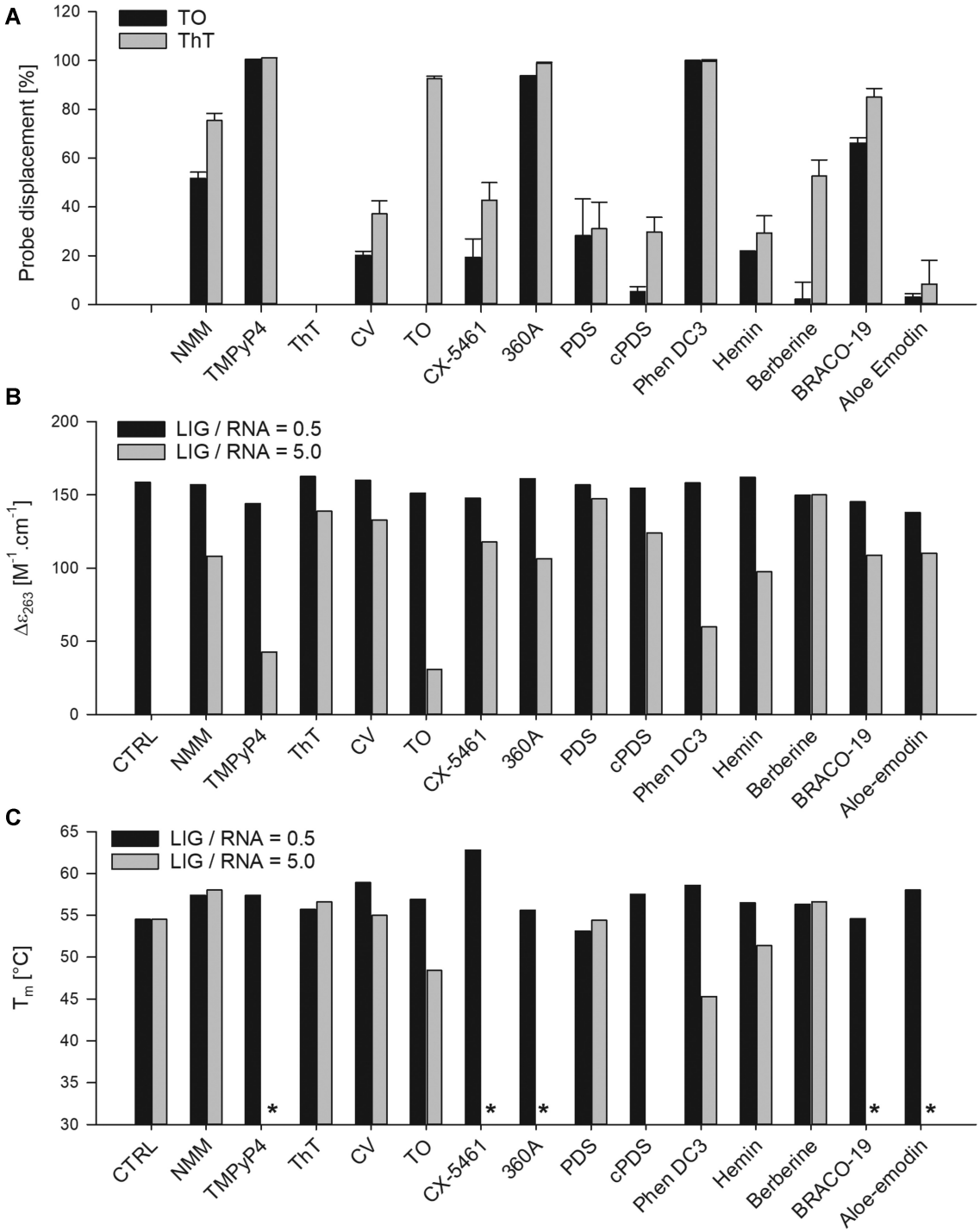

Figure 5. (**A**) Relative displacement of TO or ThT in FID experiment by various ligands. (**B**) Molar CD at 263 and (**C**) melting temperatures of TBEV-5 alone (CTRL) and in the presence of ligands at two different ratios after titration experiments, where TBEV-5 was titrated into a fixed amount of ligand (LIG/RNA = 0.5) or, vice versa, ligands were titrated to a fixed amount of TBEV-5 (LIG/RNA = 5.0). * Corresponds to cases where the experimental data do not allow T_m calculation.

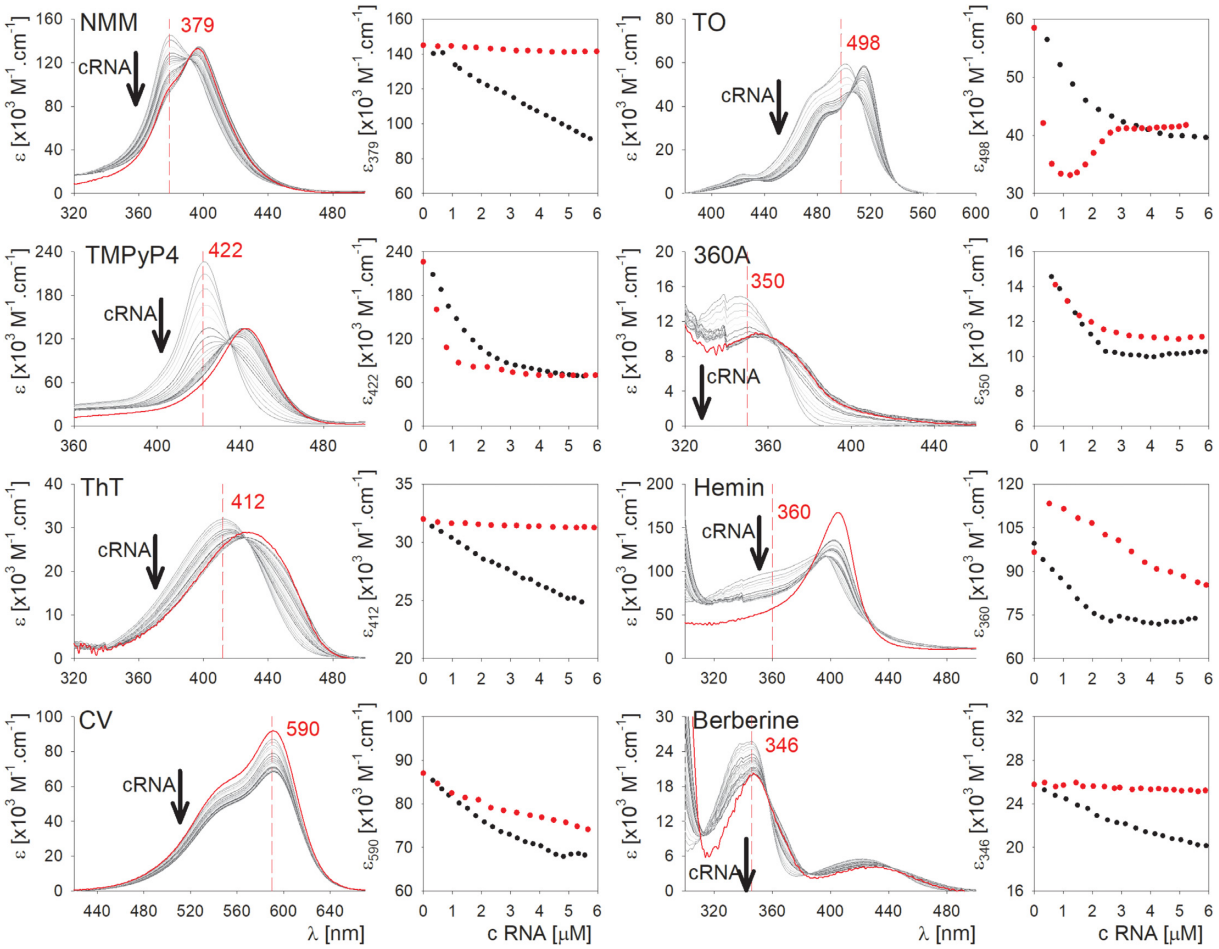

Figure 6. Molar UV absorption spectra of ligand (4 μM) with increasing concentration of TBEV-5 RNA in the ligand absorption region, measured at 23°C in 1× IC buffer and molar absorbance of ligand at selected wavelength as a function of concentration of TBEV-5 (black circles) or TBEV-5mut (red circles). Red dashed line in spectra indicates wavelength used for absorbance versus RNA concentration plot. Red spectrum corresponds to the starting spectrum from the reverse experiment, where ligand was titrated into RNA corresponding to 1:5 ligand to RNA ratio.

G4 but ThT does not displace TO at all, indicating TO as a stronger binder than ThT but with limited G4 selectivity (see above). We did not observe any significant fluorescence of TBEV-5 or TBEV-5mut alone or with any of the used ligands in the absence of TO or ThT at respective settings.

In the next step, we followed the absorbance of ligands in the visible light region upon titration with TBEV-5 and TBEV-5mut RNA (Figure 6). In the visible region, where there is no absorbance interference of the RNA, only NMM, TMPyP4, ThT, CV, TO, 360A, Hemin and berberine provide significant absorption bands and so titration data of only these ligands are presented. For CV titration, we did not observe isosbestic points that are associated with the presence of two spectral components belonging to free and bound ligands at different ratios. Moreover, the ligand-RNA interaction-induced changes in absorption of TO and, in the case of TBEV-5mut, hemin are quite complex. TBEV-5 binds all tested ligands at 4 μM concentration at the micromolar range (Figure 6) with TMPyP4 reaching 50% TBEV-5 saturation at lowest concentration, thus being the best binder. However, a control experiment with TBEV-5mut, which does not form G4, showed that TMPyP4, TO, and 360A provide similar titration curves and thus bind non-specifically. We identified NMM, ThT, berberine and hemin as ligands that specifically bind G4, though the concentration necessary for 50% saturation of TBEV-5 G4 is higher than in case of TMPyP4, indicating lower binding affinity. A reverse experiment where the ligand was gradually titrated into a fixed amount of RNA (Supplementary Figure S8) confirmed these results. The absorption spectra of the fully bound ligand (Figure 6) were observed during the reverse experiment at which the ligand to RNA ratio was around 5 to 1. Precise determination of the dissociation constant and binding stoichiometry for all ligands was impossible due to the complex absorbance changes upon titration of some ligands with TBEV-5 or insignificant absorbance changes after titration with mutated variant TBEV-5mut at the selected ranges of concentrations.

After the titration experiments we measured CD spectra of TBEV-5 and TBEV-5mut in the presence of ligands (Supplementary Figures S8 and S9) to see whether the ligands disrupt G4 formed by TBEV-5 or support G4 formation, possibly also in the case of TBEV-5mut. For the RNA-to-Ligand experiment (Figure 6), the final ratio of ligand

to RNA was 1 to 2, whereas for the Ligand-to-RNA experiment (Supplementary Figure S8), the final ratio of ligand to RNA was 5 to 1. For simplicity, we express only CD at 263 nm (Figure 5B). At 5-times ligand excess, all ligands except berberine and, to a lesser extent, ThT, CV, and PDS, decrease CD at 263 nm, indicating G4 structure alterations. The effect is most pronounced for TMPyP4, TO, and PhenDC3. At 1:2 ligand to RNA ratio, only small changes in CD were observed. Ligands do not cause significant changes in the CD of TBEV-5mut that could be attributed to induction of the G4 formation (Supplementary Figure S9).

Finally, we determined the stability of TBEV-5 G4 in the presence of interacting ligands. At 5-times molar excess of ligand, mild stabilization, represented by an increase in T_m up to 3.5°C, was observed only for NMM, ThT and berberine, i.e. ligands previously identified as specific G4 binders (Figure 5C). 360A seems to significantly increase T_m as well but the melting curve is partially distorted and the observed stabilization is not convincing. The other ligands either destabilize TBEV-5 or cause a strong distortion of melting curves, as in the case of BRACO-19, CX-5461, PhenDC3, TO, cPDS, aloe-emodin and TMPyP4. At 1:2 ligand to RNA ratio, all ligands except PDS and BRACO-19 moderately increase melting temperature by no more than 5°C. We did not observe any sigmoidal melting curves expressed from the absorbance at 297 nm for TBEV-5mut in the presence of any of the tested ligands (Supplementary Figure S10). This confirms the CD data and indicates that none of the ligands can induce G4 formation on the altered sequence.

Recently, BRACO-19 and TMPyP4 were shown to specifically interact with RNA G4 derived from the Nipah virus (67) and ZIKV genomes (17). The reported specificity of TMPyP4 towards RNA G4 contrasts with our results (Figure 6).

Activity of flaviviral RNA-dependent RNA polymerase in the presence of G4 ligands and on mutated TBEV-5 templates

The generally expected mechanism of action of the G4 ligands is based on the stabilization of viral genomic G4s, which impedes the progress of viral polymerase and causes viral replication errors. We therefore tested the effect of selected G4 ligands of flaviviral RNA-dependent-RNA-polymerase, in our case derived from the Japanese encephalitis virus, to synthesize the complementary strand. For this study, we limited the repertoire of used ligands, based on the results presented in the previous chapter, to: NMM, which is a selective and good G4 binder; PDS and cPDS, both excellent G4 binders according to the FID assay; berberine, reported antiviral compound with modest G4-binding ability and good selectivity; PhenDC3, a very strong G4 binder and TMPyP4, the most widely used G4 ligand as a reference with excellent G4 affinity, though G4 non-specific. All ligands were tested at 50, 10 and 2 μM concentrations. Besides the wild-type template (*WT*) containing the TBEV-5 sequence, we prepared for the experiment three mutant variants (Figure 7A). The *positive* mutant has four U to G substitutions and one G to A, resulting in a sequence with a $G_3NG_4N_4G_3NG_3$ pattern that is able to form a three-tetrad G4 of substantial thermodynamic stability (68). The *negative* mutant has three G to A substitutions, compared to the wild-type, resulting in a $G_2NG_2N_7G_2NG_2$ pattern, still theoretically able to fold into a two-tetrad monomolecular G4. The repertoire of codons for glycine, however, does not allow the introduction of more G4-destabilizing mutations. Positive and negative mutants code for synonymous codons as wild-type and therefore do not alter the amino acid sequence of the subsequent translation product. The *super-negative* mutant contains one more G to C substitution, compared to the negative, resulting in further disruption of one G2 block but at the expense of the change of a codon from Gly to Ala. It has to be noted that even though the synonymous codons code for the same amino acid, the usage of these codons, as well as the amount of corresponding tRNAs etc. might differ. This should not affect the *in vitro* polymerase stop assay but might somehow influence subsequent biological assays. As a reference experiment, we performed an analogous polymerase stop assay involving commercial reverse transcriptase (RT) SuperScript IV that was described to stall on RNA G4 in template strands (69). The activity of enzymes is measured as a ratio of full product of the new strand synthesis to the total labelled DNA or RNA and normalized to the control experiment with no ligand.

Using a *wild-type* template we observed around 1% of labelled primer extended by polymerase into a full product RNA (Figure 7B, Supplementary Figure S11 and S12). All tested ligands significantly inhibited RdRp synthesis of RNA in a concentration dependent manner (Figure 7C, Supplementary Figure S11). PhenDC3, PDS, cPDS and TMPyP4 reduce the activity to <10% of the no-ligand control even at 2 μM ligand concentration. NMM decreases the activity to around 15% at 50 and 10 μM and 35% at 2 μM. Berberine has strong inhibitory effect only at 50 μM concentration but at 10 and 2 μM >50% of the RdRp activity is retained. In control experiment with reverse transcriptase, we observed with *wild-type* template around 30% of labelled primer converted into a full product DNA (Figure 7D, Supplementary Figure S13 and S14). The reverse transcription experiment confirmed the most pronounced inhibitory activity of PhenDC3 ranging from a reduction to <10% at 50 μM ligand to 40% at 2 μM and a modest inhibitory effect of PDS and cPDS between reduction to <10% and 25% at 50 μM of PDS or cPDS, respectively and 60–70% at 2 μM ligand (Figure 7E, Supplementary Figure S13). NMM and TMPyP4 inhibits reverse transcriptase only at 50 μM and berberine does not inhibit RT even at 50 μM concentration. TMPyP4 at 50 μM concentration causes the formation of a smear on denaturing PAGE of the RdRp products that prevents correct quantification of the RdRp activity. We did not observe any such smear on the denaturing PAGE of RT products.

Using a *positive* template led to almost complete inhibition of full product synthesis by RdRp, even in the control experiment (Figure 7B), i.e. irrespectively of the presence of any ligand. In the case of reverse transcription on the *positive* template, we observed a reduction of full product ratio from 40% to 15%, i.e. by more than 50%, compared to the *wild-type* template (Figure 7D). Moreover, the RT on the *positive* template is much more sensitive to the

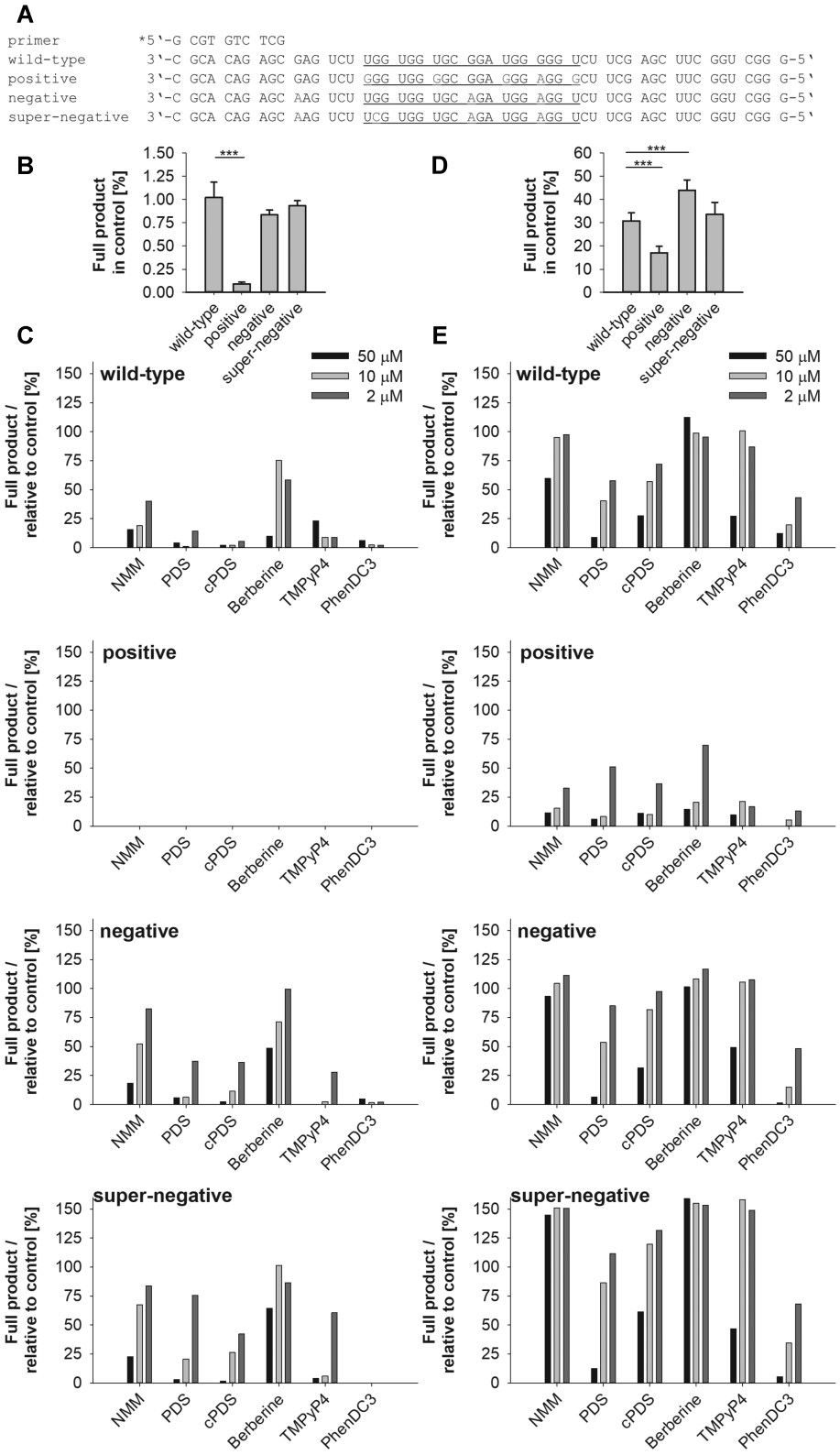

Figure 7. Fraction of full products of the polymerization reaction using four different templates (**A**), catalyzed by Japanese encephalitis virus RdRp (**B** and **C**) or SuperScript IV reverse transcriptase (**D** and **E**), in the presence of three concentrations (50, 10 and 2 μM) of six tested G4 ligands. (A) Primer and templates used for polymerase reactions. Underlining indicates TBEV-5 region. Red letters indicate nucleoside substitutions relative to wild-type. In case of JEV RdRp a RNA variant of primer, with U instead of T, was used. (B and D) Relative ratio of full product within whole control lane in JEV RdRp (B) and SuperScript IV (D) reactions. (C and E) Relative amount of full product in the presence of different concentrations of various G4 ligands normalized to the amount in control sample (no ligands). Data in panels (B) and (D) represent mean ± SD from three-four independent experiments. ***$P < 0.001$ (unpaired *t*-test).

presence of ligands. We observed a reduction in full product synthesis to less than 20%, compared to no-ligand control, for all samples except the lowest (2 μM) concentration of NMM, PDS, cPDS and berberine. The results of RdRp on *negative* and *super-negative* templates are quite similar. We did not observe significant change in full product fraction, compared to the *wild-type* template (Figure 7B). Interestingly, PhenDC3 still almost completely inhibits the activity of RdRp on both templates which might indicate inhibitory effects unrelated to the formation of G4 though no significant effect of PhenDC3 on HCV RdRp when using a non-G4 template has been reported (12). Compared to the *wild-type* template, all other ligands have a much lower inhibitory effect on RdRp synthesis at 10 and 2 μM concentration but still almost fully prevent RNA synthesis at 50 μM. The RdRp inhibitory effect is lowest in case of berberine and NMM where the ratio of full product reaches 70–100% of the control. Reference experiments with RT (Figure 7E) confirmed the strong inhibitory effect of PhenDC3 even at 10 μM concentration and PDS at 50 μM. cPDS and TMPyP4 significantly inhibits RT only at 50 μM, but at 10 and 2 μM concentrations no reduction or even increase of full product synthesis was observed. NMM and berberine did not inhibit RT even at 50 μM concentration on negative and super-negative templates. Interestingly, with RT we observed significant increase in full product fraction with *negative* template but not with the *super-negative* one, when compared to the *wild-type* template (Figure 7D).

Because the TBEV is a typical vector-borne pathogen, we took into account that TBEV replication occurs not only at 37°C in mammal hosts, but also at a considerably lower temperature in tick cells. We tested the RdRp activity also at 28°C and 20°C and we added two RNA templates that were derived from TBEV-3 and TBEV-6 regions (Supplementary Figure S15A); i.e. representing quadruplexes with lower thermodynamic stability, compared to TBEV-5 *wild-type*. First, our RdRp cannot efficiently synthesize RNA at 20°C (Supplementary Figure S12 and S15B). At 28°C the fraction of full product RNA is still reduced, compared to the reaction performed at 37°C, but the relative ratio of full product RNA between reaction with *wild-type*, *positive*, *negative* and *super-negative* template is similar to that at 37°C. Interestingly, the template derived from the TBEV-3 region does not allow efficient synthesis of RNA with RdRp even at 37°C. Control experiment with reverse transcriptase (Supplementary Figure S14 and S15C), however, clearly shows that TBEV-3 template allows synthesis of DNA. We thus hypothesize that the TBEV-3 template, or the nascent product might form and alternative structural motif that can be efficiently overcome by reverse transcriptase but not by flaviviral RdRp. TBEV-6 derived template behaves comparably to the TBEV-5 *wild-type* one.

In conclusion, our results indicate that the activity of flaviviral RdRp is strongly inhibited by the presence of G4 and can be further modulated by small-molecule ligands. The ability of G4 ligands to inhibit RdRp activity does not correlate with the G4 selectivity of the ligands but with their ability to bind RNA, including non-G4-forming variants. This might indicate G4-nonspecific inhibitory effects.

The effect of G4-ligands on TBEV replication

Based on our observation that the studied G4 ligands interacted with G4s derived from the TBEV genome sequence, we next explored their ability to suppress TBEV replication in cell-based systems. To study the biological properties of G4 ligands, we firstly evaluated the influence of the ligands on cell viability to determine their cytotoxicity for PS cells. Cytotoxicities of the G4 ligands were studied after 48-h cultivation in the presence of the compound concentration range of 0–50 μM. Notably, TO and CV displayed the highest cytotoxicity of all compounds tested and were characterized by CC_{50} values <2 μM (Figure 8A, Table 2). Relatively high cytotoxicities were also observed for CX-5461 and ThT, which showed CC_{50} values of <15 μM (Figure 8A, Table 2). These compounds were therefore excluded from further antiviral analyses. The observed cytotoxicities could be ascribed to a low selectivity of G4 ligands toward viral versus cellular G4s; these compounds could bind and (de)stabilize cellular G4s resulting in a significant decrease in cell proliferation and metabolic activity. A low selectivity of G4 ligands results from their molecular structure: most G4 ligands are composed of a large planar aromatic core that stacks on the G tetrad, reducing the probability of discrimination / recognition among different G4s (4). On the other hand, PDS, cPDS, NMM, TMPyP4, hemin, 360A, PhenDC3, BRACO-19, berberine and aloe emodin exerted good cytotoxicity profiles when used for PS cell treatment and their CC_{50} values exceeded the highest tested concentration (>50 μM) (Figure 8A, Table 2). Notably, we determined that PS cells treated with 50 μM of NMM displayed observable changes in cell morphology and in mechanical monolayer cohesion, although the metabolic activity and viability of the cells were not altered. Based on this finding, we used a maximal NMM concentration of 25 μM for all further *in vitro* experiments (apart from 50 μM as it was used for other G4 ligands). The G4 ligands with no/negligible cytotoxicity were selected for subsequent studies of ligand-mediated anti-TBEV activity.

A series of ten G4 ligands previously observed to show low cytotoxicity for PS cells was initially evaluated for their anti-TBEV potency in PS monolayers. In this initial screening, all compounds were tested against two TBEV strains Neudoerfl and Hypr, at a single concentration of 50 μM 48 h.p.i. We observed that hemin, 360A, BRACO-19 and aloe emodin (at 50 μM) showed no virus inhibition effects *in vitro* (Figure 8B). Our results with BRACO-19 contrast with results observed for the ZIKV virus, another member of the *Flavivirus* genus (17) where BRACO-19 was reported to decrease ZIKV virus titers at 100 μM concentration significantly. It is likely that these G4 ligands display poor cellular up-take into PS cells, as reported for numerous compounds having high molecular weights and/or protonated side chains on their molecules (4). Alternatively, they could be rapidly inactivated/degraded by cellular catabolism enzymes. As such, these mechanisms could be attractive targets for further investigation.

In contrast, PDS, cPDS NMM, TMPyP4, PhenDC3 and berberine suppressed replication of both TBEV strains, which corresponded to a decline of viral titers 10^2 to 10^4-fold compared with control cells (Figure 8B). The most sub-

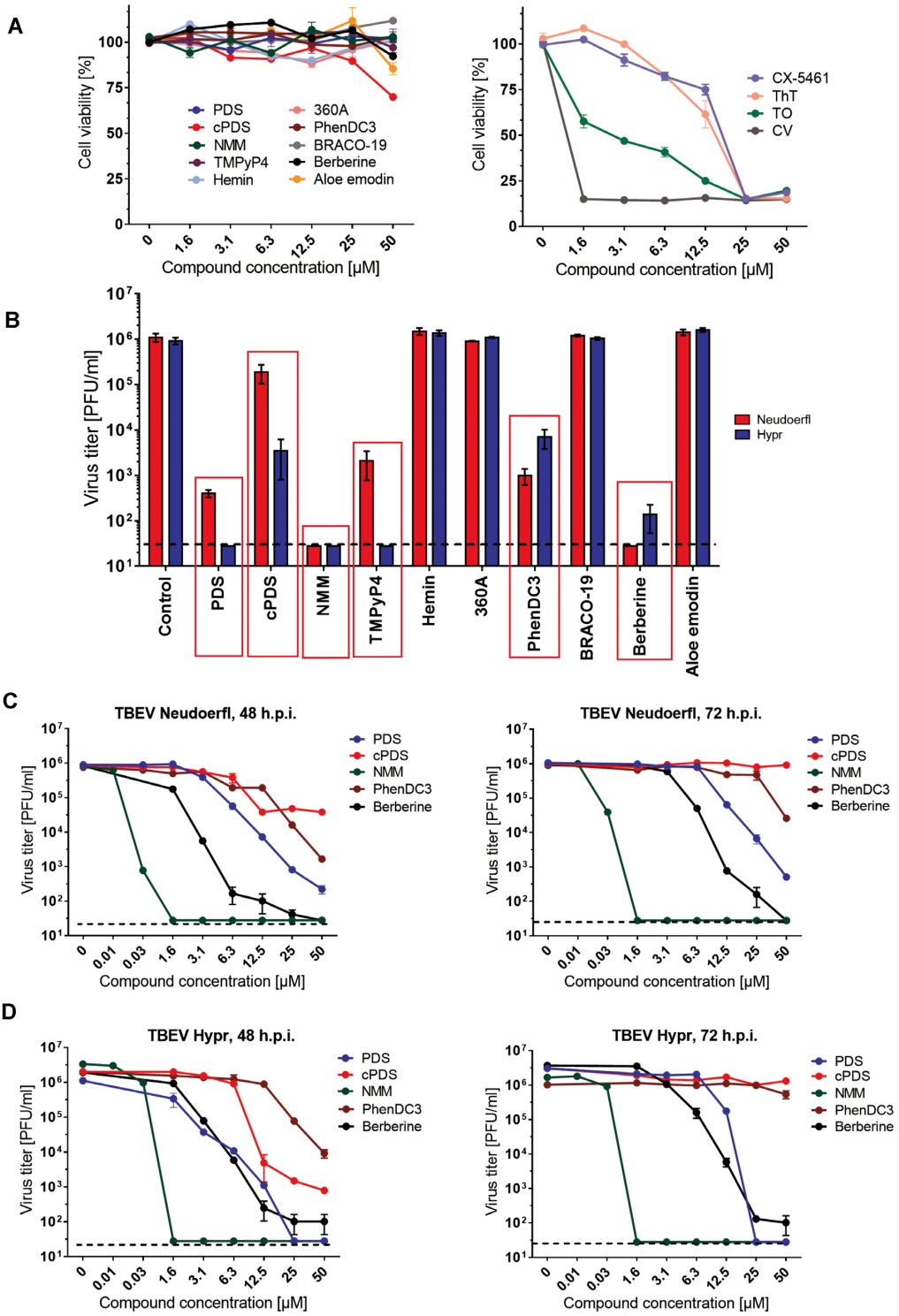

Figure 8. Antiviral activity and cytotoxicity of G4 ligands in cell-based assays. (**A**) Cytotoxicity of the indicated G4-ligands for porcine kidney stable (PS) cells determined in a concentration range of 0–50 μM and expressed as a percentage of cell viability. PS cells were seeded in 96-well plates for 24 h, then treated with G4 ligands and incubated for 48 h. (**B**) Inhibition of TBEV replication by the indicated G4-ligands. PS cell monolayers were treated with the indicated G4 ligands (50 μM) and simultaneously infected with TBEV strains Neudoerfl and Hypr at MOI of 0.1. The infected cells were then incubated with the compounds for 48 h. Following incubation, media supernatants were collected and viral titers were determined using a plaque assay and expressed as PFU/ml. Compounds PDS, cPDS, NMM, TMPyP4, berberine and PhenDC3 (marked in red) were selected for further evaluation of their antiviral potencies. (**C**, **D**) The dose-dependent anti-TBEV activities of the indicated G4-ligands were determined for TBEV Neudoerfl (C) and Hypr (D) strains. PS cell monolayers were treated with the compounds at concentrations of 0–50 μM and infected with the respective TBEV strain at MOI of 0.1. The infected cells were then incubated with the compounds for 48 h p.i. or 72 h p.i. and viral titers were determined using the plaque assay. The mean titers from three biological replicates of two independent experiments are shown and error bars indicate standard errors of the mean ($n = 3$). The horizontal dashed line indicates the minimum detectable threshold of 1.44 $\log_{10}$ PFU/ml.

Table 2. Antiviral and cytotoxicity properties of G4-ligands incubated with virus-infected PS cells for 48 h.p.i.

	Neudoerfl		Hypr				SI (CC_{50}/EC_{50})	
G4-ligand	EC_{50} [μM] [a,b]	95% CI	EC_{50} [μM][a,b]	95% CI	CC_{50} [μM] [a,c]	95% CI	Neudoerfl	Hypr
PDS	2.94	2.80 to 3.09	1.29	0.94 to 1.77	>50	-	>17.01	>36.76
cPDS	4.45	3.40 to 5.82	5.52	4.92 to 6.20	>50	-	>11.23	>9.05
NMM	0.01	0.005 to 0.028	0.02	0.021 to 0.023	>50	-	>5000	>2 500
TMPyP4	N.D.[d]	-	N.D.[d]	-	>50	-	-	-
Hemin	>50	-	>50	-	>50	-	>1	> 1
360A	> 50	-	>50	-	>50	-	>1	>1
PhenDC3	5.77	4.82 to 6.91	5.68	4.74 to 6.81	>50	-	>8.66	>8.08
BRACO-19	>50	-	>50	-	>50	-	>1	>1
Berberin	1.26	1.08 to 1.48	1.57	1.51 to 1.64	>50	-	>39.68	>31.84
Aloe emodin	>50	-	>50	-	>50	-	>1	>1
CX5461	[e]	-	[e]	-	14.14	12.20 to 16.39	-	-
ThT	[e]	-	[e]	-	10.56	9.18 to 12.14	-	-
TO	N.D. [f]	-	N.D. [f]	-	1.80	1.43 to 2.28	N.D.	N.D.
CV	N.D. [f]	-	N.D. [f]	-	<1.60	-	N.D.	N.D.

[a]Determined from three independent experiments.
[b]Expressed as a 50% reduction in viral titers and calculated as inflection points of sigmoidal inhibitory curves, which were obtained by a nonlinear fit of transformed inhibitor concentrations versus normalized response using GraphPad Prism 7.04 (GraphPad Software, Inc., USA).
[c]Expressed as a 50% reduction in cell viability and calculated as inflection points of sigmoidal viability curves, which were obtained by a nonlinear fit of transformed inhibitor concentrations versus normalized response, see [b].
[d]We were not able to evaluate the anti-TBEV effects of TMPyP4 accurately. Repeated virus cultivations in the presence of TMPyP4 provided extremely variable results that were not consistent enough to calculate the exact EC_{50} values.
[e]No antiviral effect was observed at the lowest non-cytotoxic concentration of 5 μM.
[f]Antiviral activities of TO and CV were not determined, as both compounds were highly cytotoxic (reduction of cell viability by ≥50%) in the tested concentration range (1.6–50 μM).
N.D.; not determined

stantial anti-TBEV effect was observed for NMM (EC_{50} in nanomolar values; Table 2); this compound completely suppressed TBEV replication at 1.6 μM. Anti-TBEV activities of PDS and berberine were in low micromolar levels with the EC_{50} values ranging from 1.2 to 2.9 μM for both studied TBEV strains. Anti-TBEV activity for PDS, berberine, and NMM became stable over time and was observable in both experimental intervals, 48 and 72 h.p.i. (Figure 8C and D). Other G4 ligands, cPDS and PhenDC3, showed EC_{50} values around 5 μM. However, both compounds exerted only partial inhibitory effects on virus replication being manifested by virus titer decrease by 1.5 to 3 orders of magnitude at the highest concentration tested (50 μM). Anti-TBEV effects of cPDS and PhenDC3 gradually disappeared or dropped significantly at 72 h.p.i. Unfortunately, we were not able to evaluate the anti-TBEV effects of TMPyP4 accurately. Repeated virus cultivations in the presence of TMPyP4 provided highly variable results that were not consistent enough to calculate the exact EC_{50} values (Table 2).

Furthermore, the anti-TBEV effects of G4 ligands identified in viral titer inhibition assays were confirmed by immunofluorescence staining, which was used to evaluate the expression of TBEV surface E antigen in the infected cells (Figure 9A-D). The E protein was highly expressed in virus-infected mock-treated cells; approx. 30% and 60% of virus antigen expressing cells were observed in Neudoerfl- and Hypr-infected cells, respectively (Figure 9A-D). The relatively low percentage of virus antigen expressing cells can be attributed to the fact that the virus antigen expression was monitored at the time interval of 48 h.p.i. In this time interval, the inhibitory effects of G4 ligands were very well observable but this time was not enough for the virus to spread to all the cells in the monolayer. This was particularly true for the TBEV Neudoerfl strain which is, moreover, characterized by a considerably lower replication capacity compared with the TBEV Hypr strain (70). In contrast, we detected a highly reduced or completely suppressed viral protein E expression in cell monolayers treated with PDS, cPDS, berberine and PhenDC3 at concentrations of 10 and 50 μM, and with NMM at the concentration of 10 and 25 μM at 48 h.p.i. (approx. 5% and 2% of infected cells observed for ligand concentrations 10 and 25/50 μM, respectively, Figure 9A-D).

The inhibitory effect of the G4 ligands on TBEV replication was further demonstrated on a TBEV RNA level using RT-qPCR. All studied compounds (at concentrations of 10 and 50 μM, for NMM at concentrations of 10 and 25 μM) caused a dose-dependent reduction of viral RNA copies in the infected cell culture at 48 h.p.i. The strongest inhibitory effect was demonstrated for NMM (a complete inhibition of RNA synthesis at 25 μM for both TBEV strains) whereas the weakest inhibitory activity was observed in berberine, which, however, reduced numbers of viral RNA copies by about 40% for Hypr and 25% for Neudoerfl (Figure 9E, F). Our results clearly show that the studied G4 ligands have a direct effect on TBEV RNA replication.

We further tested the anti-TBEV activity of PDS, cPDS, berberine, PhenDC3 (at 50 μM) and NMM (at 25 μM) using an adhesion assay to demonstrate in which step of the viral replication cycle the G4 ligand-mediated inhibitory effect is exerted (Supplementary Figure S16). This assay should distinguish the compounds differing in a mechanism of antiviral action which can thus be divided into two groups: 1) compounds affecting the virus adsorption/fusion and 2) compounds acting inside the infected cells and im-

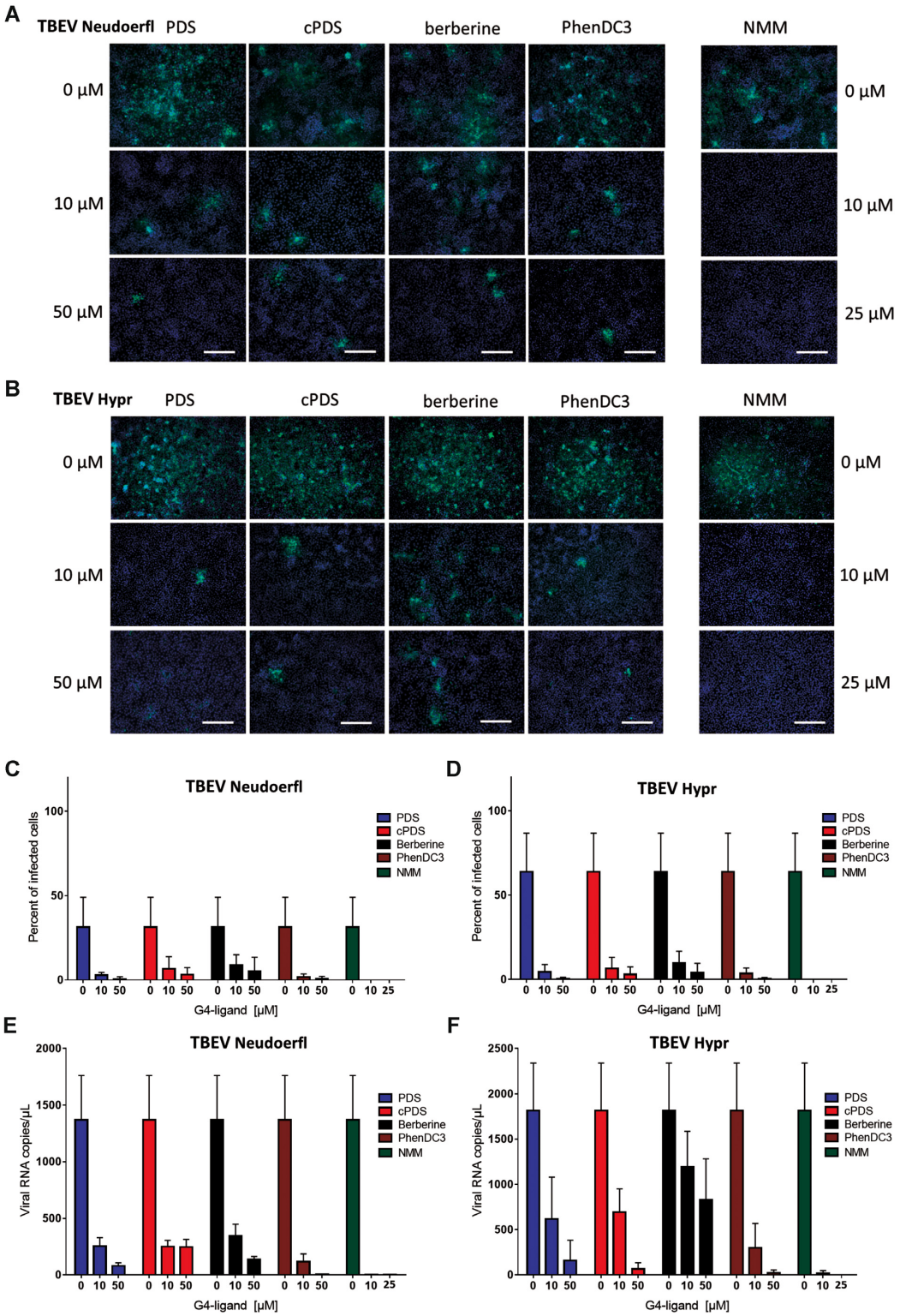

Figure 9. Inhibition of TBEV surface antigen expression and viral RNA synthesis by G4 ligands. (**A**, **B**) Fluorescence staining of PS cell culture infected with the TBEV Neudoerfl (A) and Hypr (B) strain at a MOI of 0.1 in the presence of G4 ligands at the indicated concentrations. PS cells were fixed on slides at 48 h post-infection, stained with mouse flavivirus-specific antibody as a primary antibody, and anti-mouse goat secondary antibody conjugated with with FITC (green) and counterstained with DAPI (blue). Scale bars, 200 µm. (**C**, **D**) The level of TBEV Neudoerfl (C) and Hypr (D) antigen expression in the presence of G4 ligands was quantified and expressed as a percentage of infected (viral antigen expressing) cells relative to mock-infected cells. Mean percentage of infected cells from two independent experiments are shown and error bars indicate the standard errors of the mean ($n = 3$). (**E**, **F**) The effect of G4 ligands on TBEV Neudoerfl (E) and Hypr (F) RNA copy numbers was studied using quantitative real-time PCR (RT-qPCR). The mean viral RNA copy numbers/µl are shown and error bars indicate standard errors of the mean (Neudoerfl: $n = 15$ for controls, $n = 3$ for individual ligand-treated samples; Hypr: $n = 30$ for controls, $n = 6$ for individual ligand treated samples).

pairing virus replication/assembly machinery. This assay revealed that the antiviral action of PDS, cPDS, berberine, and PhenDC3 (at 50 μM) takes effect in the post-entry/fusion phase of the viral replication cycle (mechanism 2) (Supplementary Figure S16). The mode of action of PDS was recently studied also by Zou *et al*. (18) showing that PDS is involved in the ZIKV replication period rather than entry which is in agreement with our observations. To confirm these results, we performed the transfection of the isolated viral RNA pre-treated with the selected ligands (i.e. berberine and PDS at 0, 10, 50, and 200 μM). We hypothesized that if the ligand interacts directly with the viral RNA then the transfected viral RNA pre-treated with the ligand has a decreased capacity to be replicated, transcribed or translated to form viable viral particles, being manifested by a decrease in viral titers. Indeed, after transfection of viral RNA pre-treated by berberine or PDS we observed a partial (for berberine at 0–200 μM and for PDS at 10 μM) or a complete (for PDS at 50 and 200 μM) suppression of infectious viral particle formation (Supplementary Figure S17). These results support our previous findings that berberine and PDS showed anti-TBEV activity based on the ligand-viral RNA interaction. This mechanism of action can also be expected for cPDS and PhDC3.

On the other hand, the adhesion assay showed that NMM (at 25 μM) caused virus inhibition prior to the entry/fusion steps of the viral replication cycle (mechanism 1) (Supplementary Figure S16). This is not surprising as porphyrins with negatively charged/polar site chains were previously demonstrated to incorporate into liposomes (71,72) and viral envelopes to act as viral entry/fusion inhibitors (73–76). However, it is interesting that when we transfected the viral RNA pre-treated with NMM at 25 and 200 μM, no viable viral particle formation was observed (Supplementary Figure S17). We can speculate that NMM could have multiple modes of antiviral action; 1) this compound blocks the viral entry/fusion machinery and also 2), when crossing the plasmatic membrane, interacts with viral RNA and suppresses viral genome replication. The latter hypothesis (the antiviral activity of NMM based on ligand-viral RNA interaction and G4 stabilization) was supported by our biophysical results as well as by biochemical methods based on the reverse-transcriptase and/or flaviviral RdRp stalling assays. It should also be noted that porphyrins were previously described to recognize various molecular targets (76) and their biological activities can be associated, in addition to interacting with G4s and viral/liposomal membranes, also with heme metabolism impairment and heme oxygenase inhibition (77–79) and photodynamic inactivation of pathogens via reactive oxygen species generation (80–82).

Other examples of multiple modes of action for G4 ligands were reported for berberine and related benzylisoquinoline alkaloids, which were described not only to interact with nucleic acids and inhibit nucleic acid synthesis and reverse transcriptase activity (83), but also could regulate signaling pathways based on MEK-ERK, NF-kB and AMPK/mTOR, which are necessary for viral replication (84). The multiple mode of action was recently demonstrated also for PDS. This compound, in addition to the G4 stabilization, interacts with ZIKV NS2B-NS3 protease and reduces its catalytic activity (18). Taken together, molecular mechanisms of antiviral activities for many G4 ligands appear to be more complex, making it difficult to link and correlate directly the results obtained using biophysical, biochemical, and biological methodological approaches.

Phenotype properties of recombinant TBEV mutated in the TBEV-5 region

To address the question if G4 structures are relevant to virus replication, a site-directed mutagenesis approach (Figure 10A) was used to introduce conformation-specific mutations into the TBEV-5 sequence of recombinant TBEV variants (Figure 10B). The selected mutations reflect those used for an *in vitro* study of flaviviral RdRp in the previous chapter on TBEV-5 sequence (Figure 7A). Thus, after transfection of the subgenomic fragments into permissive BHK-21 cells, the following recombinant TBEV variants (G4-specific TBEV mutants) were successfully rescued: 1) the *positive* TBEV mutant (T7653G/G7656A/T7659G/T7665G/T7671G) forming a highly stabilized quadruplex within the TBEV-5 sequence. 2) The *negative* mutant (G7656A/G7662A/G7677A) with an impaired ability to fold TBEV-5 quadruplex. 3) The *super-negative* mutant (G7656A/G7662A/G7670C/G7677A) with a completely abolished TBEV-5 quadruplex formation. Finally, 4) the recombinant wild-type virus with no introduced mutations in the TBEV-5 sequence (Figure 10B). As mentioned above, all mutations were synonymous and their introduction did not result in amino acid substitution apart from the only exception of the G2A amino acid substitution in the NS5 gene of the *super-negative* mutant. This substitution was, however, necessary for the complete destabilization of the TBEV-5 quadruplex. As G2A represents a substitution for a structurally/functionally similar amino acid and because it is located outside of the methyltransferase or RdRp active sites we are convinced that this change does not significantly affect the NS5 activity.

To characterize the phenotypic properties of the obtained G4-specific TBEV mutants *in vitro*, the growth kinetics and plaque morphology of the recombinant mutated viruses were assayed in PS cells and compared with wild-type (Figure 11). The recombinant wild-type virus amplified in PS cells (MOI of 0.1) showed a short lag period within the interval from 0 to 18 h p.i. Starting 24 h p.i., the wild-type TBEV exerted an exponential increase in virus infectivity reaching a peak titer of 4.2×10^6 PFU/ml within 72 h p.i. and gradually declining thereafter (Figure 11A).

The *positive* mutant cultured in PS cells at MOI of 0.1 showed a substantially decreased replication fitness (Figure 11A), which was manifested by viral titers 1–1.5 orders of magnitude lower than the wild-type within the intervals 24–96 h p.i. After 96 h of cultivation in PS cells, the *positive* TBEV mutant reached a peak titer of 4.6×10^5 PFU/ml. The strongly altered replication fitness of the *positive* TBEV mutant was even more pronounced, when PS cells were infected with this mutated virus at MOI of 0.01 (Figure 11B). Importantly, the decreased replication capacity of the *positive* TBEV mutant resulted also in dramatic changes in plaque morphology; this mutated virus formed

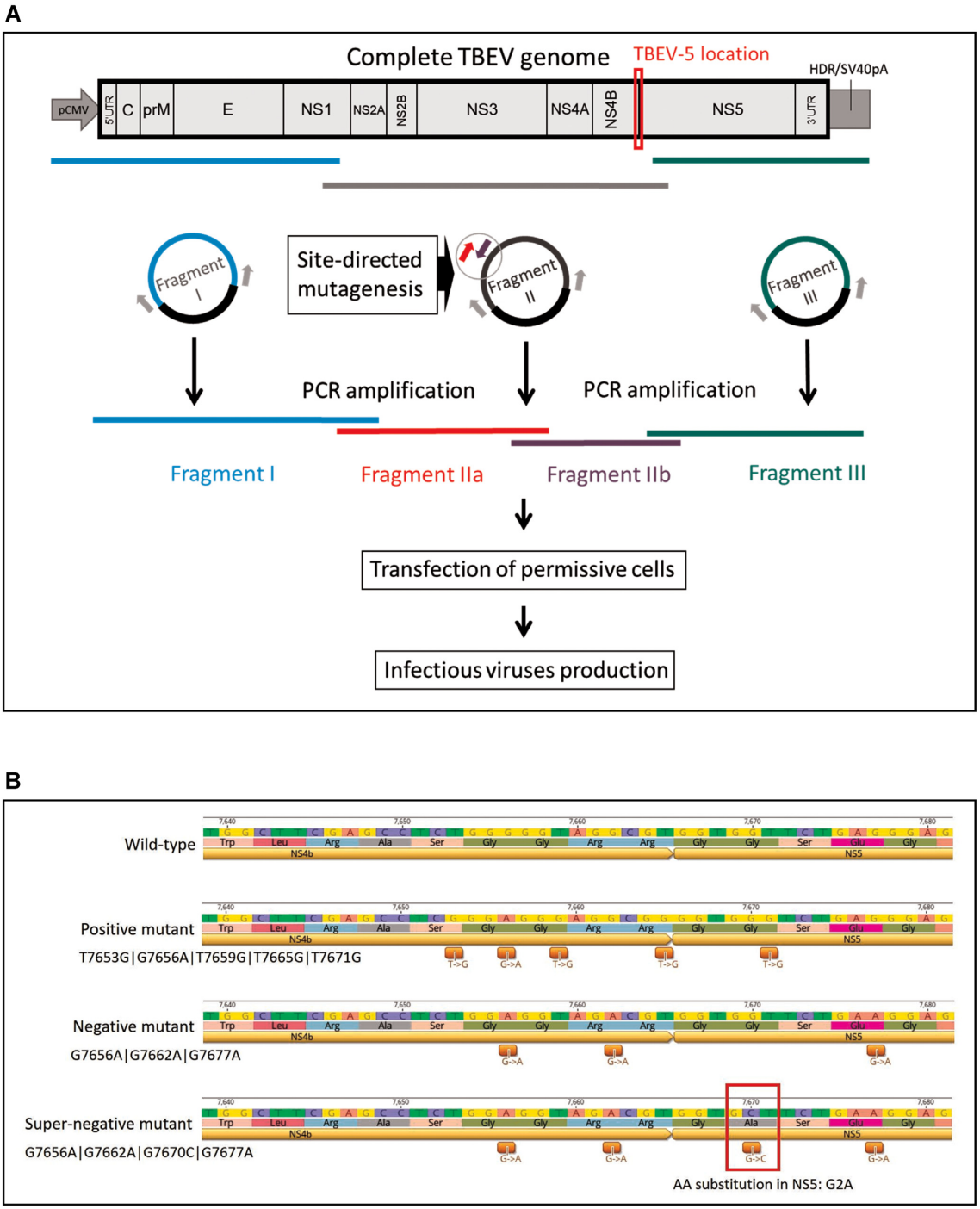

Figure 10. Site-directed mutagenesis to form recombinant TBEV mutated in the TBEV-5 region. (**A**) Schematic representation of the reverse-genetics system used in this study. The reverse-genetics system was based on the generation of infectious subgenomic overlapping DNA fragments that encompass the entire viral genome. Three de novo-synthesized DNA fragments (I, II and III) cloned into a pUC57 or pC11 vectors were used. Fragment I was flanked with the human cytomegalovirus promoter (pCMV) at the 5′ end and fragment III with the hepatitis delta ribozyme, followed by the simian virus 40 polyadenylation signal (HDR/SV40pA) at the 3′end. Unmodified primers were used to generate unmodified amplicons I, II, and III (i.e. the production of wild-type virus). Mutated primers located on the targeted TBEV-5 region on fragment II were used to generate two mutated sub-amplicons IIa and IIb (red and violet) (i.e. the production of the positive, negative, and super-negative TBEV mutants). An equimolar mix of these four DNA fragments was used to transfect BHK-21 cells to obtain infectious viral particles. After transfection, the infectious viral particles were rescued and the presence of the desired mutations in the TBEV-5 region was confirmed by sequencing. (**B**) Genotypes of the recombinant TBEV mutated in the TBEV-5 region and the wild-type virus. The introduced mutations are indicated. The scheme was generated using the Geneious Prime® software, version 2021.2.2 (Biomatters, Ltd.; New Zealand).

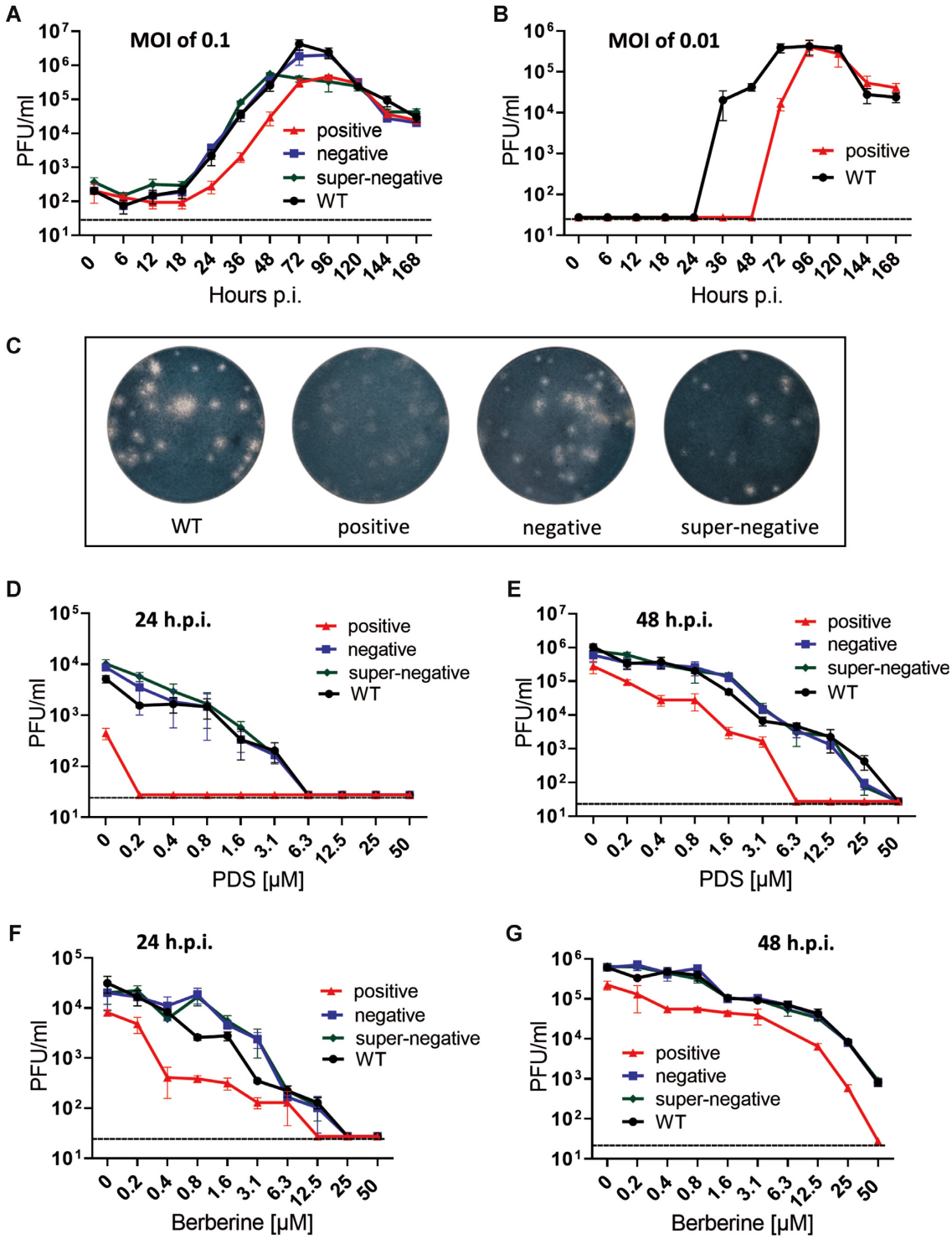

Figure 11. Phenotype properties of the recombinant TBEV mutated in the TBEV-5 sequence. (**A**) Growth kinetics of the positive, negative, and super-negative mutants, and wild-type TBEV at MOI of 0.1 within the 7-day experimental period to assess the replication efficacy of the mutant TBEV in PS cells. (**B**) Growth kinetics of the positive TBEV mutant and the wild-type virus at MOI of 0.01 within the 7-day experimental period in PS cells. (**C**) Plaque morphology of G4-specific TBEV mutants was assessed in PS cell monolayers and compared to the wild-type virus. (**D**, **E**) The sensitivity profiles of the positive, negative, and super-negative TBEV mutants to PDS were evaluated in PS cells and compared to the corresponding wild-type TBEV at 24 h p.i. (D) and 48 h p.i. (E). (**F**,**G**) The sensitivity profiles of G4-speficic TBEV mutants to berberine were evaluated in PS cells and compared to the corresponding wild-type TBEV at 24 h p.i. (F) and 48 h p.i. (G) Experiments were performed in three biological replicates. The mean titers are shown, and error bars indicate the standard errors of the mean. The horizontal dashed line indicates the minimum detectable threshold of 1.44 $\log_{10}$ PFU/ml.

turbid (cloudy) and indistinct plaques, compared with large and clear plaques of the wild-type (Figure 11C). The sequence analysis of the *positive* TBEV mutant revealed the partial reverse of the mutated TBEV-5 sequence to the wild-type genotype, as both mutated and reverted genotypes were identified in RNA samples isolated from the supernatant media after a 168-h cultivation of the *positive* TBEV mutant in PS cells (Supplementary Table S3). The reverted genotype was determined in one from three analyzed RNA samples and, moreover, in this RNA sample the reversals occurred only in the positions T7653G, T7659G, T7665G and T7671G. The mutation at position 7656 was retained. These observations clearly indicate that the high stabilization of the TBEV-5 G4 resulted in a strong impairment of the viral replication, which could be explained by the inhibitory effect of the stabilized G4 on the RdRp-directed RNA replication process, as was also demonstrated using the flaviviral RdRp stalling assays (see above). Thus, the *positive* TBEV mutant population was subject to a selection pressure which led to the gradual elimination of the G4-stabilizing mutations and to the restoration of the wild-type genotype configuration, when the mutated virus was cultivated for 168 h in cell culture.

The growth kinetics of the *negative* mutant was almost indistinguishable from the wild-type virus (Figure 11A). After a lag period (0–18 h p.i.) the *negative* TBEV mutant entered an exponential replication phase and reached a peak titer of 1.8×10^6 PFU/ml at 96 h p.i. At the end of the experiment (at 168 h p.i.), the virus titer dropped to 2.0×10^4 PFU/ml. The plaque morphology of the *negative* mutant was similar to that of the wild-type virus; both recombinant viruses produced large and clear plaques which were round and regular in shape and did not change in shape and size during all cultivation experiments (Figure 11C). Interestingly, the *negative* TBEV mutant maintained the introduced mutations during the whole cultivation experiment (for 168 h); in all analyzed RNA samples only the mutated genotype was detected (Supplementary Table S3). It is evident that destabilization of the TBEV-5 G4 in the *negative* TBEV mutant did not affect the virus replication significantly and, therefore, there was no/negligible selection pressure to eliminate the mutated TBEV-5 sequence and revert to the wild-type genotype. We suppose that the mutagenesis of multiple quadruplex forming sequences located in multiple viral genes could lead to more pronounced changes in viral replication fitness. This will be a subject of our future research.

The replication fitness of the *super-negative* TBEV mutant was also similar to that of wild-type (Figure 11A). The similarity in replication kinetics was most pronounced at the intervals of 0 to 48 h p.i. The *super-negative* TBEV mutant reached the peak titer of 5.6×10^5 PFU/ml at 48 h p.i. In later phases of cultivation in PS cells, the replication of the *super-negative* TBEV mutant gradually declined to 4.3×10^4 PFU/ml. The plaque morphology of the *super-negative* mutant was indistinguishable from plaques formed by the negative mutant and wild-type (Figure 11C). Notably, a complete reversion to the wild-type genotype was observed, after the *super-negative* TBEV mutant was cultured in PS cells for 168 h (only mutation G7677A was retained in one of the analyzed samples, Supplementary Table S3). The extensive impairment to fold G4 in TBEV-5 was probably highly disadvantageous for virus replication in cell culture and therefore, there was a strong selection pressure to completely eliminate the introduced conformation-specific mutations afterwards. The rapid reversion to the wild-type genotype could also explain the similar phenotype properties of the *super-negative* mutant and the wild-type virus.

Finally, we investigated the sensitivity of the G4-specific TBEV mutants to two selected G4 ligands (PDS and berberine, concentration range from 0 to 50 μM). We examined the dose-dependent effect of both ligands on virus replication at two cultivation periods (24 and 48 h p.i.). The growth curves of the *negative* and *super-negative* TBEV mutants cultivated in the presence of PDS exerted very similar shapes and slopes as that of the wild-type (Figure 11D, E). Replication of the three recombinant viruses were completely inhibited at the compound concentration of 6.3 μM at 24 h p.i. and 50 μM at 48 h p.i., demonstrating no substantial differences in sensitivities of the *negative* and *super-negative* TBEV mutants and wild-type to PDS. These results are not surprising given that the replication fitness of the *negative* and *super-negative* mutants are similar with that of the wild-type virus. In a sharp contrast, however, the *positive* mutant exhibited an increased sensitivity to PDS compared to the wild-type virus and to both *negative* and *super-negative* mutants. At 24 h p.i. virus replication was completely suppressed even at the minimal PDS concentration tested (0.2 μM). The increased sensitivity of the *positive* TBEV mutant was clearly apparent also after a 48-h cultivation; the growth curve of the *positive* mutant had a markedly steep slope and the mutated virus was completely inhibited at the PDS concentration of 6.3 μM (Figure 11D, E). Similar results, although less pronounced, were obtained also when the mutated viruses and the wild-type TBEV were cultured in the presence of berberine at both cultivation intervals (24 and 48 h p.i.) (Figure 11F, G).

CONCLUSIONS

In this study, we predicted seven potential G4 forming sequences in the RNA genome of TBEV located in the C, NS1, NS4b and NS5 genes and the 3′-UTR. The ability to form stable monomolecular G4 was confirmed by biophysical methods for five of the potential G4 forming sequences. All observed G4s were parallel stranded. With the NS4b/NS5 derived G4 (TBEV-5), the best hit in terms of phylogenetic conservation and G4 properties, we observed strong interactions with selected small molecule-based G4 ligands, which were later demonstrated to show low cytotoxicity and potent antiviral efficacies against TBEV in cell-based systems. PDS, cPDS, NMM, TMPyP4, PhenDC3 and berberine also caused the suppression of viral surface E protein expression and the decrease in viral RNA copy numbers in virus-infected PS cell culture. While PDS and berberine showed detectable antiviral effects only in the late phase of the TBEV life cycle, NMM exerted an inhibitory effect also in the early steps (entry/fusion) of TBEV replication. Thus, it is evident that even well-characterized G4-binding ligands can affect different stages of the viral replication cycle and may recognize multiple viral/host molecular targets, other than G4s alone. The observed antiviral

effect of such compounds could then be the result of partial inhibition processes at different levels of the viral replication cycle. Moreover, the TBEV mutant forming a highly stabilized monomolecular TBEV-5 quadruplex (the *positive* mutant) showed a substantially decreased replication capability, altered plaque morphology and increased susceptibility to selected G4 ligands. From the mechanistic point of view, the alterations in TBEV phenotype mutated in the TBEV-5 region can be explained by the G4-mediated inhibition of viral RNA synthesis, as also demonstrated using the *in vitro* flaviviral RdRp stalling assay. In contrast, the TBEV mutants with destabilized TBEV-5 quadruplexes (the *negative* and *super-negative* mutants) showed no phenotype differences compared with the wild-type virus. The *super-negative* mutant, moreover, exerted a rapid reversal to the wild-type genotype. Our results indicate that there is a stability threshold for G4 sequences located in the RNA genome of TBEV and that mutational shift from this stability threshold to form strongly (de)stabilized G4s is severely penalized, either by viral replication fitness decrease or by rapid reversion back to this optimal level of G4 stability. The findings of our study represent a solid base for new directions in the drugability of tick-borne encephalitis, present G4s in the TBEV RNA genome as prospective targets for novel small molecule-based drugs, which bind G4 structures, alter their stability and disrupt the viral replication cycle.

SUPPLEMENTARY DATA

Supplementary Data are available at NAR Online.

FUNDING

Czech Science Foundation [20-20229S to D.Re., L.E.]; SYMBIT [CZ.02.1.01/0.0/0.0/15_003/0000477] financed from the ERDF; EU Horizon 2020 [653316 (EVAg)]. Funding for open access charge: Czech Science Foundation [20-20229S].
Conflict of interest statement. None declared.

REFERENCES

1. Neidle,S. and Balasubramanian,S. (2006) In: *Quadruplex Nucleic Acids*. Royal Society of Chemistry, London, Cambridge.
2. Huppert,J.L. and Balasubramanian,S. (2005) Prevalence of quadruplexes in the human genome. *Nucleic Acids Res.*, **33**, 2908–2916.
3. Varshney,D., Spiegel,J., Zyner,K., Tannahill,D. and Balasubramanian,S. (2020) The regulation and functions of DNA and RNA G-quadruplexes. *Nat. Rev. Mol. Cell Biol.*, **21**, 459-474.
4. Ruggiero,E. and Richter,S.N. (2018) G-quadruplexes and G-quadruplex ligands: targets and tools in antiviral therapy. *Nucleic Acids Res.*, **46**, 3270–3283.
5. Bohálová,N., Cantara,A., Bartas,M., Kaura,P., Šťastný,J., Pečinka,P., Fojta,M., Mergny,J.L. and Brázda,V. (2021) Analyses of viral genomes for G-quadruplex forming sequences reveal their correlation with the type of infection. *Biochimie*, **186**, 13–27.
6. Artusi,S., Nadai,M., Perrone,R., Biasolo,M.A., Palù,G., Flamand,L., Calistri,A. and Richter,S.N. (2015) The herpes simplex virus-1 genome contains multiple clusters of repeated G-quadruplex: implications for the antiviral activity of a G-quadruplex ligand. *Antiviral Res.*, **118**, 123–131.
7. Murat,P., Zhong,J., Lekieffre,L., Cowieson,N.P., Clancy,J.L., Preiss,T., Balasubramanian,S., Khanna,R. and Tellam,J. (2014) G-quadruplexes regulate epstein-barr virus-encoded nuclear antigen 1 mRNA translation. *Nat. Chem. Biol.*, **10**, 358–364.
8. Gilbert-Girard,S., Gravel,A., Artusi,S., Richter,S.N., Wallaschek,N., Kaufer,B.B. and Flamand,L. (2017) Stabilization of telomere G-Quadruplexes interferes with human herpesvirus 6A chromosomal integration. *J. Virol.*, **91**, e00402–17.
9. Perrone,R., Nadai,M., Poe,J.A., Frasson,I., Palumbo,M., Palù,G., Smithgall,T.E. and Richter,S.N. (2013) Formation of a unique cluster of G-quadruplex structures in the HIV-1 nef coding region: implications for antiviral activity. *PLoS One*, **8**, e73121.
10. Wang,S.-R., Zhang,Q.-Y., Wang,J.-Q., Ge,X.-Y., Song,Y.-Y., Wang,Y.-F., Li,X.-D., Fu,B.-S., Xu,G.-H., Shu,B. *et al.* (2016) Chemical targeting of a G-Quadruplex RNA in the ebola virus l gene. *Cell Chem. Biol.*, **23**, 1113–1122.
11. Wang,S.-R., Min,Y.-Q., Wang,J.-Q., Liu,C.-X., Fu,B.-S., Wu,F., Wu,L.-Y., Qiao,Z.-X., Song,Y.-Y., Xu,G.-H. *et al.* (2016) A highly conserved G-rich consensus sequence in hepatitis c virus core gene represents a new anti-hepatitis c target. *Sci. Adv.*, **2**, e1501535.
12. Jaubert,C., Bedrat,A., Bartolucci,L., Di Primo,C., Ventura,M., Mergny,J.-L., Amrane,S. and Andreola,M.-L. (2018) RNA synthesis is modulated by G-quadruplex formation in hepatitis c virus negative RNA strand. *Sci. Rep.*, **8**, 8120–8120.
13. Bian,W.-X., Xie,Y., Wang,X.-N., Xu,G.-H., Fu,B.-S., Li,S., Long,G., Zhou,X. and Zhang,X.-L. (2019) Binding of cellular nucleolin with the viral core RNA G-quadruplex structure suppresses HCV replication. *Nucleic Acids Res.*, **47**, 56–68.
14. Luo,X., Xue,B., Feng,G., Zhang,J., Lin,B., Zeng,P., Li,H., Yi,H., Zhang,X.-L., Zhu,H. *et al.* (2019) Lighting up the native viral RNA genome with a fluorogenic probe for the live-cell visualization of virus infection. *J. Am. Chem. Soc.*, **141**, 5182–5191.
15. Fleming,A.M., Ding,Y., Alenko,A. and Burrows,C.J. (2016) Zika virus genomic RNA possesses conserved G-Quadruplexes characteristic of the flaviviridae family. *ACS Infect. Dis.*, **2**, 674–681.
16. Fleming,A.M., Nguyen,N.L.B. and Burrows,C.J. (2019) Colocalization of m(6)A and G-Quadruplex-Forming sequences in viral RNA (HIV, zika, hepatitis b, and SV40) suggests topological control of adenosine N(6)-Methylation. *ACS Central Sci.*, **5**, 218–228.
17. Majee,P., Pattnaik,A., Sahoo,B.R., Shankar,U., Pattnaik,A.K., Kumar,A. and Nayak,D. (2021) Inhibition of zika virus replication by G-quadruplex-binding ligands. *Mol. Ther. Nucleic Acids*, **23**, 691–701.
18. Zou,M., Li,J.Y., Zhang,M.J., Li,J.H., Huang,J.T., You,P.D., Liu,S.W. and Zhou,C.Q. (2021) G-quadruplex binder pyridostatin as an effective multi-target ZIKV inhibitor. *Int. J. Biol. Macromol.*, **190**, 178–188.
19. Abiri,A., Lavigne,M., Rezaei,M., Nikzad,S., Zare,P., Mergny,J.-L. and Rahimi,H.-R. (2021) Unlocking G-Quadruplexes as antiviral targets. *Pharmacol. Rev.*, **73**, 897–923.
20. Ruggiero,E., Zanin,I., Terreri,M. and Richter,S.N. (2021) G-Quadruplex targeting in the fight against viruses: an update. *Int. J. Mol. Sci.*, **22**, 10984.
21. Ruzek,D., Avšič Županc,T., Borde,J., Chrdle,A., Eyer,L., Karganova,G., Kholodilov,I., Knap,N., Kozlovskaya,L., Matveev,A. *et al.* (2019) Tick-borne encephalitis in europe and russia: review of pathogenesis, clinical features, therapy, and vaccines. *Antiviral Res.*, **164**, 23–51.
22. Deviatkin,A.A., Karganova,G.G., Vakulenko,Y.A. and Lukashev,A.N. (2020) TBEV subtyping in terms of genetic distance. *Viruses*, **12**, 1240.
23. Füzik,T., Formanová,P., Růžek,D., Yoshii,K., Niedrig,M. and Plevka,P. (2018) Structure of tick-borne encephalitis virus and its neutralization by a monoclonal antibody. *Nat. Commun.*, **9**, 436–436.
24. Edgar,R.C. (2004) MUSCLE: multiple sequence alignment with high accuracy and high throughput. *Nucleic Acids Res.*, **32**, 1792–1797.
25. Okonechnikov,K., Golosova,O., Fursov,M. and team, t.U. (2012) Unipro UGENE: a unified bioinformatics toolkit. *Bioinformatics*, **28**, 1166–1167.
26. Kikin,O., D'Antonio,L. and Bagga,P.S. (2006) QGRS mapper: a web-based server for predicting G-quadruplexes in nucleotide sequences. *Nucleic Acids Res.*, **34**, W676–W682.
27. Hon,J., Martínek,T., Zendulka,J. and Lexa,M. (2017) pqsfinder: an exhaustive and imperfection-tolerant search tool for potential quadruplex-forming sequences in R. *Bioinformatics*, **33**, 3373–3379.
28. Bedrat,A., Lacroix,L. and Mergny,J.-L. (2016) Re-evaluation of G-quadruplex propensity with G4Hunter. *Nucleic Acids Res.*, **44**, 1746–1759.

29. Garant,J.-M., Perreault,J.-P. and Scott,M.S. (2017) Motif independent identification of potential RNA G-quadruplexes by G4RNA screener. *Bioinformatics*, **33**, 3532–3537.
30. Lacroix,L. (2019) G4HunterApps. *Bioinformatics*, **35**, 2311–2312.
31. Crooks,G.E., Hon,G., Chandonia,J.M. and Brenner,S.E. (2004) WebLogo: a sequence logo generator. *Genome Res.*, **14**, 1188–1190.
32. Kejnovska,I., Renciuk,D., Palacky,J. and Vorlickova,M. (2019) In: Yang,D. and Lin,C. (eds). *G-Quadruplex Nucleic Acids: Methods and Protocols*. Humana Press Inc, Totowa, Vol. **2035**, pp.25–44.
33. Rodriguez,R., Müller,S., Yeoman,J.A., Trentesaux,C., Riou,J.-F. and Balasubramanian,S. (2008) A novel small molecule that alters shelterin integrity and triggers a DNA-damage response at telomeres. *J. Am. Chem. Soc.*, **130**, 15758–15759.
34. Travascio,P., Bennet,A.J., Wang,D.Y. and Sen,D. (1999) A ribozyme and a catalytic DNA with peroxidase activity: active sites versus cofactor-binding sites. *Chem. Biol.*, **6**, 779–787.
35. Chung,W.J., Heddi,B., Hamon,F., Teulade-Fichou,M.P. and Phan,A.T. (2014) Solution structure of a G-quadruplex bound to the bisquinolinium compound phen-dc(3). *Angew. Chem. Int. Ed. Engl.*, **53**, 999–1002.
36. Mohanty,J., Barooah,N., Dhamodharan,V., Harikrishna,S., Pradeepkumar,P.I. and Bhasikuttan,A.C. (2013) Thioflavin t as an efficient inducer and selective fluorescent sensor for the human telomeric G-quadruplex DNA. *J. Am. Chem. Soc.*, **135**, 367–376.
37. Monchaud,D., Allain,C. and Teulade-Fichou,M.P. (2006) Development of a fluorescent intercalator displacement assay (G4-FID) for establishing quadruplex-DNA affinity and selectivity of putative ligands. *Bioorg. Med. Chem. Lett.*, **16**, 4842–4845.
38. Kong,D.M., Ma,Y.E., Wu,J. and Shen,H.X. (2009) Discrimination of G-quadruplexes from duplex and single-stranded DNAs with fluorescence and energy-transfer fluorescence spectra of crystal violet. *Chemistry*, **15**, 901–909.
39. Gowan,S.M., Harrison,J.R., Patterson,L., Valenti,M., Read,M.A., Neidle,S. and Kelland,L.R. (2002) A G-quadruplex-interactive potent small-molecule inhibitor of telomerase exhibiting in vitro and in vivo antitumor activity. *Mol. Pharmacol.*, **61**, 1154–1162.
40. Wang,S., Yan,W.W., He,M., Wei,D., Long,Z.J. and Tao,Y.M. (2020) Aloe emodin inhibits telomerase activity in breast cancer cells: transcriptional and enzymological mechanism. *Pharmacol. Rep.*, **72**, 1383–1396.
41. Franceschin,M., Rossetti,L., D'Ambrosio,A., Schirripa,S., Bianco,A., Ortaggi,G., Savino,M., Schultes,C. and Neidle,S. (2006) Natural and synthetic G-quadruplex interactive berberine derivatives. *Bioorg. Med. Chem. Lett.*, **16**, 1707–1711.
42. Arthanari,H., Basu,S., Kawano,T.L. and Bolton,P.H. (1998) Fluorescent dyes specific for quadruplex DNA. *Nucleic Acids Res.*, **26**, 3724–3728.
43. Yett,A., Lin,L., Beseiso,D., Miao,J. and Yatsunyk,L. (2019) N-methyl mesoporphyrin IX as a highly selective light-up probe for G-quadruplex DNA. *J. Porphyrins Phthalocyanines*, **23**, 1195–1215.
44. Izbicka,E., Wheelhouse,R.T., Raymond,E., Davidson,K.K., Lawrence,R.A., Sun,D.Y., Windle,B.E., Hurley,L.H. and Von Hoff,D.D. (1999) Effects of cationic porphyrins as G-quadruplex interactive agents in human tumor cells. *Cancer Res.*, **59**, 639–644.
45. Di Antonio,M., Biffi,G., Mariani,A., Raiber,E.A., Rodriguez,R. and Balasubramanian,S. (2012) Selective RNA versus DNA G-quadruplex targeting by in situ click chemistry. *Angew. Chem. Int. Ed. Engl.*, **51**, 11073–11078.
46. Rocca,R., Talarico,C., Moraca,F., Costa,G., Romeo,I., Ortuso,F., Alcaro,S. and Artese,A. (2017) Molecular recognition of a carboxy pyridostatin toward G-quadruplex structures: why does it prefer RNA? *Chem. Biol. Drug Des.*, **90**, 919–925.
47. Granotier,C., Pennarun,G., Riou,L., Hoffschir,F., Gauthier,L.R., De Cian,A., Gomez,D., Mandine,E., Riou,J.F., Mergny,J.L. *et al.* (2005) Preferential binding of a G-quadruplex ligand to human chromosome ends. *Nucleic Acids Res.*, **33**, 4182–4190.
48. Xu,H., Di Antonio,M., McKinney,S., Mathew,V., Ho,B., O'Neil,N.J., Santos,N.D., Silvester,J., Wei,V., Garcia,J. *et al.* (2017) CX-5461 is a DNA G-quadruplex stabilizer with selective lethality in BRCA1/2 deficient tumours. *Nat. Commun.*, **8**, 14432–14432.
49. Tran,P.L., Largy,E., Hamon,F., Teulade-Fichou,M.P. and Mergny,J.L. (2011) Fluorescence intercalator displacement assay for screening G4 ligands towards a variety of G-quadruplex structures. *Biochimie*, **93**, 1288–1296.
50. Carvalho,J., Lopes-Nunes,J., Paula Cabral Campello,M., Paulo,A., Milici,J., Meyers,C., Mergny,J.L., Salgado,G.F., Queiroz,J.A. and Cruz,C. (2020) Human papillomavirus G-Rich regions as potential antiviral drug targets. *Nucleic Acid Ther.*, **31**, 68–81.
51. Mergny,J.L. and Lacroix,L. (2003) Analysis of thermal melting curves. *Oligonucleotides*, **13**, 515–537.
52. Kozuch,O. and Mayer,V. (1975) Pig kidney epithelial (PS) cells: a perfect tool for the study of flaviviruses and some other arboviruses. *Acta Virol.*, **19**, 498.
53. Aubry,F., Nougairède,A., de Fabritus,L., Querat,G., Gould,E.A. and de Lamballerie,X. (2014) Single-stranded positive-sense RNA viruses generated in days using infectious subgenomic amplicons. *J. Gen. Virol.*, **95**, 2462–2467.
54. Driouich,J.S., Ali,S.M., Amroun,A., Aubry,F., de Lamballerie,X. and Nougairède,A. (2018) SuPReMe: a rapid reverse genetics method to generate clonal populations of recombinant RNA viruses. *Emerg. Microbes Infect.*, **7**, 40.
55. Eyer,L., Nougairède,A., Uhlířová,M., Driouich,J.S., Zouharová,D., Valdés,J.J., Haviernik,J., Gould,E.A., De Clercq,E., de Lamballerie,X. *et al.* (2019) An E460D substitution in the NS5 protein of tick-borne encephalitis virus confers resistance to the inhibitor galidesivir (BCX4430) and also attenuates the virus for mice. *J. Virol.*, **93**, e00367-19.
56. De Madrid,A.T. and Porterfield,J.S. (1969) A simple micro-culture method for the study of group b arboviruses. *Bull. World Health Organ.*, **40**, 113–121.
57. Eyer,L., Valdés,J.J., Gil,V.A., Nencka,R., Hřebabecký,H., Šála,M., Salát,J., Černý,J., Palus,M., De Clercq,E. *et al.* (2015) Nucleoside inhibitors of tick-borne encephalitis virus. *Antimicrob. Agents Chemother.*, **59**, 5483–5493.
58. Konkolova,E., Dejmek,M., Hřebabecký,H., Šála,M., Böserle,J., Nencka,R. and Boura,E. (2020) Remdesivir triphosphate can efficiently inhibit the RNA-dependent RNA polymerase from various flaviviruses. *Antiviral Res.*, **182**, 104899.
59. Lu,G., Bluemling,G.R., Collop,P., Hager,M., Kuiper,D., Gurale,B.P., Painter,G.R., De La Rosa,A. and Kolykhalov,A.A. (2017) Analysis of ribonucleotide 5′-Triphosphate analogs as potential inhibitors of zika virus RNA-Dependent RNA polymerase by using nonradioactive polymerase assays. *Antimicrob. Agents Chemother.*, **61**, e01967-16.
60. Niyomrattanakit,P., Abas,S.N., Lim,C.C., Beer,D., Shi,P.Y. and Chen,Y.L. (2011) A fluorescence-based alkaline phosphatase-coupled polymerase assay for identification of inhibitors of dengue virus RNA-dependent RNA polymerase. *J. Biomol. Screen*, **16**, 201–210.
61. Sáez-Álvarez,Y., Arias,A., Del Águila,C. and Agudo,R. (2019) Development of a fluorescence-based method for the rapid determination of zika virus polymerase activity and the screening of antiviral drugs. *Sci. Rep.*, **9**, 5397.
62. Lavezzo,E., Berselli,M., Frasson,I., Perrone,R., Palù,G., Brazzale,A.R., Richter,S.N. and Toppo,S. (2018) G-quadruplex forming sequences in the genome of all known human viruses: a comprehensive guide. *PLoS Comput. Biol.*, **14**, e1006675.
63. Puig Lombardi,E. and Londoño-Vallejo,A. (2019) A guide to computational methods for G-quadruplex prediction. *Nucleic Acids Res.*, **48**, 1603.
64. Islam,B., Stadlbauer,P., Vorlíčková,M., Mergny,J.L., Otyepka,M. and Šponer,J. (2020) Stability of two-quartet G-Quadruplexes and their dimers in atomistic simulations. *J. Chem. Theory Comput.*, **16**, 3447–3463.
65. Kejnovská,I., Stadlbauer,P., Trantírek,L., Renčiuk,D., Gajarský,M., Krafčík,D., Palacký,J., Bednářová,K., Šponer,J., Mergny,J.-L. *et al.* (2021) G-Quadruplex formation by DNA sequences deficient in guanines: two tetrad parallel quadruplexes do not fold intramolecularly. *Chem. Eur. J.*, **27**, 12115–12125.
66. Kypr,J., Kejnovska,I., Renciuk,D. and Vorlickova,M. (2009) Circular dichroism and conformational polymorphism of DNA. *Nucleic Acids Res.*, **37**, 1713–1725.
67. Majee,P., Kumar Mishra,S., Pandya,N., Shankar,U., Pasadi,S., Muniyappa,K., Nayak,D. and Kumar,A. (2020) Identification and characterization of two conserved G-quadruplex forming motifs in the nipah virus genome and their interaction with G-quadruplex specific ligands. *Sci. Rep.*, **10**, 1477.
68. Zhang,A.Y.Q., Bugaut,A. and Balasubramanian,S. (2011) A sequence-independent analysis of the loop length dependence of

intramolecular RNA G-quadruplex stability and topology. *Biochemistry*, **50**, 7251–7258.
69. Kwok,C.K., Marsico,G., Sahakyan,A.B., Chambers,V.S. and Balasubramanian,S. (2016) rG4-seq reveals widespread formation of G-quadruplex structures in the human transcriptome. *Nat. Methods*, **13**, 841.
70. Wallner,G., Mandl,C.W., Ecker,M., Holzmann,H., Stiasny,K., Kunz,C. and Heinz,F.X. (1996) Characterization and complete genome sequences of high- and low- virulence variants of tick-borne encephalitis virus. *J. Gen. Virol.*, **77**, 1035–1042.
71. Kepczyński,M. and Ehrenberg,B. (2002) Interaction of dicarboxylic metalloporphyrins with liposomes. The effect of pH on membrane binding revisited. *Photochem. Photobiol.*, **76**, 486–492.
72. Kepczyński,M., Pandian,R.P., Smith,K.M. and Ehrenberg,B. (2002) Do liposome-binding constants of porphyrins correlate with their measured and predicted partitioning between octanol and water? *Photochem. Photobiol.*, **76**, 127–134.
73. Assuncao-Miranda,I., Cruz-Oliveira,C., Neris,R.L.S., Figueiredo,C.M., Pereira,L.P.S., Rodrigues,D., Araujo,D.F.F., Da Poian,A.T. and Bozza,M.T. (2016) Inactivation of dengue and yellow fever viruses by heme, cobalt-protoporphyrin IX and tin-protoporphyrin iX. *J. Appl. Microbiol.*, **120**, 790–804.
74. Cruz-Oliveira,C., Almeida,A.F., Freire,J.M., Caruso,M.B., Morando,M.A., Ferreira,V.N.S., Assuncao-Miranda,I., Gomes,A.M.O., Castanho,M. and Poian,Da, A.T. (2017) Mechanisms of vesicular stomatitis virus inactivation by protoporphyrin IX, zinc-protoporphyrin IX, and mesoporphyrin iX. *Antimicrob. Agents Chemother.*, **61**, 14.
75. Man,D., Slota,R., Broda,M.A., Mele,G. and Li,J. (2011) Metalloporphyrin intercalation in liposome membranes: ESR study. *J. Biol. Inorg. Chem.*, **16**, 173–181.
76. Neris,R.L.S., Figueiredo,C.M., Higa,L.M., Araujo,D.F., Carvalho,C.A.M., Vercoza,B.R.F., Silva,M.O.L., Carneiro,F.A., Tanuri,A., Gomes,A.M.O. *et al.* (2018) Co-protoporphyrin IX and Sn-protoporphyrin IX inactivate zika, chikungunya and other arboviruses by targeting the viral envelope. *Sci. Rep.*, **8**, 13.
77. Schmidt,W.N., Mathahs,M.M. and Zhu,Z.W. (2012) Herne and HO-1 inhibition of HCV, HBV, and HIV. *Front. Pharmacol.*, **3**, 13.
78. Chung,S.W., Hall,S.R. and Perrella,M.A. (2009) Role of haem oxygenase-1 in microbial host defence. *Cell. Microbiol.*, **11**, 199–207.
79. Wegiel,B., Nemeth,Z., Correa-Costa,M., Bulmer,A.C. and Otterbein,L.E. (2014) Heme oxygenase-1: a metabolic nike. *Antioxid. Redox. Signal.*, **20**, 1709–1722.
80. Costa,L., Faustino,M.A.F., Neves,M., Cunha,A. and Almeida,A. (2012) Photodynamic inactivation of mammalian viruses and bacteriophages. *Viruses-Basel*, **4**, 1034–1074.
81. Pushpan,S.K., Venkatraman,S., Anand,V.G., Sankar,J., Parmeswaran,D., Ganesan,S. and Chandrashekar,T.K. (2002) Porphyrins in photodynamic therapy - a search for ideal photosensitizers. *Curr. Med. Chem. Anticancer Agents*, **2**, 187–207.
82. Wiehe,A., O'Brien,J.M. and Senge,M.O. (2019) Trends and targets in antiviral phototherapy. *Photochem. Photobiol. Sci.*, **18**, 2565–2612.
83. Maiti,M. and Kumar,G.S. (2010) Polymorphic nucleic acid binding of bioactive isoquinoline alkaloids and their role in cancer. *J. Nucleic Acids*, **2010**, https://doi.org/10.4061/2010/593408.
84. Warowicka,A., Nawrot,R. and Gozdzicka-Jozefiak,A. (2020) Antiviral activity of berberine. *Arch. Virol.*, **165**, 1935–1945.